CSNAP, the smallest CSN subunit, modulates proteostasis through cullin-RING ubiquitin ligases

Maria G. Füzesi-Levi[a], Radoslav Ivanov Enchev[b], Gili Ben-Nissan[a], Yishai Levin[c], Meital Kupervaser[c], Gilgi Friedlander[d], Tomer Meir Salame[e], Reinat Nevo[a], Matthias Peter[b], and Michal Sharon[a]

[a]Department of Biomolecular Sciences, Weizmann Institute of Science, Rehovot Israel
[b]ETH Zurich, Department of Biology, Institute of Biochemistry, Zurich, Switzerland
[c]Nancy and Stephen Grand Israel National Center for Personalized Medicine, Weizmann Institute of Science, Rehovot, Israel
[d]Ilana and Pascal Mantoux Institute for Bioinformatics, and Nancy and Stephen Grand Israel National Center for Personalized Medicine, Weizmann Institute of Science, Rehovot, Israel.
[e]Flow Cytometry Unit, Weizmann Institute of Science, Rehovot, Israel

Corresponding author:
Michal Sharon
Tel: (+972)-8-934-3947
Fax: (+972)-8-934-6010
Email: michal.sharon@weizmann.ac.il

Abstract

The cullin–RING ubiquitin E3 ligase (CRL) family consists of ~250 complexes that catalyze ubiquitylation of proteins to achieve cellular regulation. All CRLs are inhibited by the COP9 signalosome complex (CSN) through both enzymatic (deneddylation) and non-enzymatic (steric) mechanisms. The relative contribution of these two mechanisms is unclear. Here, we decouple the mechanisms using CSNAP, the recently discovered ninth subunit of the CSN. We find that CSNAP reduces the affinity of CSN toward CRL complexes. Removing CSNAP does not affect deneddylation, but leads to global effects on the CRL, causing altered reproductive capacity, suppressed DNA damage response, decreased viability, and delayed cell cycle progression. Thus, although CSNAP is only 2% of the CSN mass, it plays a critical role in the steric regulation of CRLs by the CSN.

Introduction

Protein degradation is one of the essential mechanisms that enables reshaping of the proteome landscape in response to various stimuli (Hershko, Ciechanover et al., 2000). The specificity of this process is largely mediated by E3 ligases that ubiquitinate target proteins (Deshaies & Joazeiro, 2009, Enchev, Schulman et al., 2015). One of the largest E3 ubiquitin ligase families, responsible for ubiquitination of 20% of the proteins degraded by the 26S proteasome, is comprised of cullin-RING ligases (CRLs) (Soucy, Smith et al., 2009). This family encompasses ~ 250 distinct complexes that are built in a modular fashion around a central cullin scaffold, which is associated with a specific substrate receptor, adaptor protein, and a RING protein that recruits the E2 enzyme (reviewed in (Deshaies & Joazeiro, 2009, Skaar, Pagan et al., 2013)). Seven different cullins have been identified in humans, each interacting with a dedicated set of receptors, forming CRL complexes that target a single or a small group of substrate proteins. At any given time, various CRLs are active, and their dynamic assembly and disassembly enables cellular adaptation in response to regulatory inputs.

In spite of the great diversity of CRLs in terms of composition and substrate specificity, all complexes are regulated by the COP9 signalosome complex (CSN) (Deshaies & Joazeiro, 2009). The CSN regulates CRLs by means of two independent mechanisms, catalytic and non-catalytic. The first involves enzymatic deconjugation of the ubiquitin-like protein Nedd8 from the cullin subunit (deneddylation) (Cope, Suh et al., 2002). The latter is mediated through physical binding to CRLs, sterically precluding interactions with E2 enzymes and ubiquitination of substrates (Emberley, Mosadeghi et al., 2012, Enchev, Scott et al., 2012, Fischer, Scrima et al., 2011). By inhibiting CRL activity, both mechanisms control the gateway to the exchange cycle that remodels CRL composition (Liu, Reitsma et al., 2018, Mosadeghi, Reichermeier et al., 2016, Reitsma, Liu et al., 2017).

The CSN is a highly conserved complex that exists in all eukaryotes (Wei & Deng, 2003, Wei, Serino et al., 2008). Three types of subunits constitute this complex: two MPN subunits (for Mpr1p and Pad1p N terminal) CSN5 and CSN6 (Glickman, Rubin et al., 1998), six PCI subunits (for proteasome, COP9, and initiation factor 3); CSN1–CSN4, CSN7, and CSN8 (Hofmann & Bucher, 1998); and an additional small, non-PCI or MPN

subunit that we recently discovered and termed CSNAP, for CSN acidic protein (Rozen, Fuzesi-Levi et al., 2015). The CSNAP protein consists of only 57 amino acids (molecular weight: 6.2 kDa) that link together the two distinct structural elements of the CSN by mutually binding the MPN subunits CSN5 and CSN6, and the PCI subunit CSN3 (Rozen et al., 2015). Given the small size of CSNAP, a natural question that arises is whether it is actually crucial for CSN function and, if so, what is its functional role? In this study, we address these questions by combining biochemical and cell biology approaches, together with mass spectrometry analysis.

Using the above approaches, we discovered that manipulating CSNAP enables us to uncouple the steric and catalytic activities of the CSN complex. Although it is only 2% of the CSN mass, we find that removing CSNAP has a global effect on the cell cycle, cell viability and DNA damage response. This effect is due to a reduction in the K_d of CSN-CRL binding, leaving deneddylation activity unchanged. These findings provides a role for CSNAP, and points to the affinity of CSN-CRL interactions as a critical component for proteostasis.

Results

CSNAP alters the strength of CSN-CRL interaction

To investigate the impact of CSNAP on both the enzymatic and steric activities of CSN, we initially examined the complex's deneddylation activity, using HAP-1 cell lines lacking CSNAP (ΔCSNAP cells) (Rozen et al., 2015). Comparison of the deneddylated/neddylated ratio between WT and ΔCSNAP cells showed that in the absence of CSNAP there are only minor changes of less than 15% of the cullin's deneddylated fraction (Fig 1A). This result is in accordance with our previous finding, showing that WT and ΔCSNAP cells exhibit a similar rate of deneddylation (Rozen et al., 2015) and with a study that compared the rate of deneddylation of endogenous CSN prepared from HEK293 cells, with that of recombinant $CSN^{\Delta CSNAP}$ expressed in insect cells (Emberley et al., 2012, Enchev et al., 2012). Thus, it can be concluded that CSNAP does not significantly affect the catalytic capacity of the CSN complex.

To examine whether the steric activity of $CSN^{\Delta CSNAP}$ is affected by the absence of CSNAP, we applied label-free quantification of protein intensities from pull-down assays, coupled with mass spectrometry (MS) analysis of WT and ΔCSNAP cells. We reasoned that if CSNAP impacts the CSN-CRL interaction, differences in the array of protein binding partners will be revealed. Our results indicated that multiple CRL components are significantly enriched in ΔCSNAP pulldowns, in comparison to immunoprecipitation of WT cells (Fig. 1B and Table S1). These mainly include substrate receptors (DDB2, FBOX17, FBXL15 and KLH22) and adapter proteins (TCEB2, TCEB1, SKP1 and ASB6). In the WT cells, only three proteins, DCAF4, BTBD2 and BTBD1, were enriched; all are CRL substrate receptor proteins. To validate these results, we carried out reciprocal co-immunoprecipitation experiments. The results obtained for the ΔCSNAP and WT cell lines confirmed that FBXL15 and DDB2 are enriched in the $CSN^{\Delta CSNAP}$ pulldown experiment, in comparison to the WT complex (Fig. 1C). Notably, these results did not arise from changes in the expression levels of CSN subunits, as all CSN subunits (except for CSNAP, depleted from the cells) displayed insignificant differences when the two cell lines were compared (Fig. 1B), a finding that was further validated by Western blot analysis (Fig. 1D, Fig. S1). Taken together, the data suggest that CSNAP plays a role in tuning CSN-CRL interactions in cells.

To further assess the contribution of CSNAP to the CSN/CRL interaction, we utilized a quantitative *in vitro* binding assay to determine the affinity between Cul1-Rbx1, and recombinant $CSN^{\Delta CSNAP}$ or CSN complexes (Mosadeghi et al., 2016) (Fig. S2, S3). In this assay, the environmentally-sensitive dye dansyl was conjugated to the C-terminus of Cul1, and an increase in fluorescence upon CSN binding was detected (Mosadeghi et al., 2016). Both WT CSN5 and the well characterized CSN5-H138A mutant (Emberley et al., 2012, Enchev et al., 2012, Mosadeghi et al., 2016) (CSN^{5H138A}) were used, as the latter binds Cul1-Rbx1 ~30-fold more tightly, enabling us to reach saturation. The results indicate that CSN complexes display decreased affinity to Cul1-Rbx1, in comparison to $CSN^{\Delta CSNAP}$ (Fig. 1E, Fig S4). Taken together, the results imply that CSNAP reduces the affinity of the CSN towards CRL complexes.

CSNAP is required for proper cell cycle progression and viability

The apparent difference in K_d for $CSN^{\Delta CSNAP}$ binding to SCF, compared to CSN, led us to question whether such a change in affinity can influence the repertoire of active CRLs and, as a consequence, the array of ubiquitinated proteins. We therefore performed a large-scale analysis of protein ubiquitination, relying on the enrichment of ubiquitinated tryptic peptides (Udeshi, Mertins et al., 2013). The relative differences in ubiquitination of WT and ΔCSNAP cells was quantified, using the SILAC (stable isotope labeling by amino acids in cell culture) approach (Ong, Blagoev et al., 2002). The results indicated that differences exist in the extent of ubiquitination in ΔCSNAP and WT cell lines (Fig. 2A and Table S2A and B). In all, 159 ubiquitinated proteins, were found to be enriched only in WT and not in ΔCSNAP cells, while 79 ubiquitinated proteins, were abundant in cells lacking CSNAP. Of the 238 proteins whose ubiquitination levels differed between the two type of cells, 64 are known substrates of the different CRL complexes (Table S3) (Emanuele, Elia et al., 2011, Koren, Timms et al., 2018, Yen & Elledge, 2008, Zheng, Zhou et al., 2016). These results suggest that reducing the affinity between CSN and CRL modifies CRL assembly and, consequently, the repertoire of ubiquitinated proteins.

Functional annotations revealed that among the ubiquitinated proteins identified as being enriched in WT, or ΔCSNAP cells, 16% are clustered in the cell cycle pathway (Fig. 2B-C, Tables S4, S5A and S5B). We confirmed this data by assessing the cell cycle distribution of both ΔCSNAP and WT cells, using flow cytometry analysis. The results indicated that compared to WT cells, ΔCSNAP cells display larger S and G2 phase populations (Fig. 2D). This phenotype can be prevented by exogenous expression of CSNAP-Cerulean, but not by the truncated form of the protein (ΔC-CSNAP-Cerulean), which lacks the C-terminal region that is crucial for the protein's integration into the CSN (Rozen et al., 2015). In addition, colony formation assays (Franken, Rodermond et al., 2006) showed that the viability of cells lacking CSNAP is significantly reduced, in comparison to that of WT cells (Fig. 2E). Taken together, our results suggest that the absence of CSNAP influences CSN-CRL interactions in a manner that affects, protein ubiquitination and, therefore likely, cell cycle coordination.

Cellular protein levels are influenced by CSNAP

Considering the dependence of the ubiquitinated proteome on the presence of CSNAP, we wished to examine whether the impact of this subunit would also be detected in a global proteome analysis. To this end, we performed label-free quantification (Shalit, Elinger et al., 2015) of the proteomes of WT and ΔCSNAP cells. Given that the CSN complex and protein ubiquitination are vital to the DNA damage response (Dubois, Gerber et al., 2016, Fuzesi-Levi, Ben-Nissan et al., 2014, Hannss & Dubiel, 2011, Meir, Galanty et al., 2015), we performed the analysis both prior to and following exposure of the cells to UV irradiation. Data were analyzed by two-way ANOVA, taking into consideration both the UV treatment, and the type of cell being treated (WT or ΔCSNAP). Proteins that were considered significantly differentially expressed were clustered into five groups according to their cellular functions (Fig. 3A and Tables S6A-D and S7). Remarkably, we noticed that cellular pathways that were enriched in this experiment are in accordance with those identified in the SILAC-based ubiquitinylation analysis (Fig. 2B-C). Among these proteins we could identify known substrates of various CRL complexes (Table S8), which are known to be involved in ubiquitination, apoptosis, cell cycle regulation and DNA damage response. This observation may explain the detected phenotypic effects.

Examination of the five clusters indicated that even under normal conditions, there are clear differences in protein expression levels among WT and ΔCSNAP cells. A particularly striking observation was that the cellular response to UV irradiation was nearly abolished in ΔCSNAP cells (Fig. 3B). We validated the proteomics results by Western blot analysis to monitor the expression levels of four proteins that displayed differential expression levels between WT and ΔCSNAP cells: the quinone reductase enzyme, NQO1, the tumor suppressor PDCD4, and the filament protein vimentin, which appear in Cluster 4, and PARP1, a member of the PARP family that appears in Cluster 3 (Fig. 3A; see arrows on the right). The results confirmed that unlike WT cells, NQO1, PDCD4, and vimentin are expressed at high levels in ΔCSNAP cells (Fig. 3C and S5). Likewise, the blots validated that the expression of PARP1 in WT cells is high under normal conditions, and is decreased following UV-induced DNA damage; while in ΔCSNAP cells, regardless of UV irradiation, low levels of PARP1 expression are maintained (Fig. 3C and S5). We also

noticed that in WT cells, a cleavage product of PARP1 was detected, a phenomenon that was not observed in ΔCSNAP cells; this result will be further discussed in the next section. In summary, our findings suggest that the lack of CSNAP following UV-treatment elicited a strong and specific influence on downstream effectors of the DNA damage response.

CSNAP is required for DNA repair

Building on our results reflecting the compromised protein remodeling capability following DNA damage in ΔCSNAP cells, we wished to explore the DNA repair response in these cells. Initially, we measured the DNA repair capacity following UV irradiation using the comet assay (Olive & Banath, 2006). The results indicated that ΔCSNAP cells display a longer tail moment, which is associated with the accumulation of both single- and double-strand DNA breaks (Fig. 4A). Following DNA damage, cells would reduce their rates of proliferation, in order to enable DNA damage repair (Gentile, Latonen et al., 2003). We therefore measured cell proliferation before and after treatment with UV irradiation, and found that, as expected, proliferation arrest was detected in WT cells, however, not in cells lacking CSNAP, nor in ΔCSNAP cells exogenously expressing ΔC-CSNAP-Cerulean, which is not incorporated into the CSN complex (Fig. 4B). Nevertheless, cell rescue was achieved in ΔCSNAP cells by overexpressing the full-length CSNAP protein.

Considering that widespread DNA damage induces cell cycle arrest (Gentile et al., 2003), we evaluated the cell cycle distribution of WT and ΔCSNAP cells exposed to UV irradiation following a double thymidine block, which induces a G1/S-phase arrest. After their release from cell cycle synchronization, untreated ΔCSNAP cells proceeded to the S phase significantly more slowly than WT cells, and reached the G2 phase with a delay of approximately four hours (Fig. 4C). However, following the induction of DNA damage, CSNAP-depleted cells, unlike the WT cells that displayed a slight delay in progression, remained stalled in the S and G2 phases. This scenario could be due to impaired checkpoint control, rather than exclusively due to a faulty DNA repair mechanism. We therefore validated that the activation of the UV-induced kinase, Chk1, is not dependent on CSNAP, (Figure S6). Similarly, comparison of the colony-forming potential of WT and ΔCSNAP cells following UV irradiation, indicated a significant, 2.7-fold reduction in the number of colonies of cells lacking CSNAP (Fig. 4D). This finding suggests that the accumulation of

damaged DNA compromises cell cycle progression and reproductive ability in ΔCSNAP cells.

Next, we determined whether the absence of CSNAP affects DNA damage-induced cellular apoptosis. To this end, we measured the populations of live, early apoptotic and late apoptotic cells in UV-exposed WT and ΔCSNAP cultures four hours post-damage, using flow cytometry. We found that the population of early apoptotic cells following UV exposure is significantly enlarged in WT cells (Fig. 4E), a phenomenon that does not occur at that time point in ΔCSNAP cells, suggesting that the latter fail to efficiently activate the early apoptotic response as WT cells.

Cleavage of PARP1 by caspases is considered to be a hallmark of apoptosis (Chaitanya, Steven et al., 2010, Kaufmann, Desnoyers et al., 1993, Soldani & Scovassi, 2002), and in agreement with the above results, a cleavage product of the protein was detected only in WT but not in ΔCSNAP cells (Fig. 3C). To further examine this phenomenon, we monitored the appearance of the 89 kDa cleavage product of PARP1 following UV irradiation, in a time-dependent manner. We found that in WT cells, the presence of the 89 kDa fragment could already be detected 1 hour following DNA damage (Fig. 4F, Fig. S7). The levels of the cleavage product increased over time, concomitantly with the reduction of the full-length PARP1 (113 kDa) protein. In ΔCSNAP cells, however, the relative abundance of PARP1 was lower than in WT cells, even prior to UV irradiation, and the formation of the 89 kDa cleavage product was only detected after 6.5 hours. Therefore, delayed PARP1 cleavage in ΔCSNAP cells may explain the inability of these cells to activate the early apoptotic response.

Previous studies have shown that CSN is physically recruited to DNA damage sites on the chromatin, and on its path partners with $CUL4A^{DDB2}$ (Fuzesi-Levi et al., 2014, Groisman, Polanowska et al., 2003, Meir et al., 2015). The CSN/ $CUL4A^{DDB2}$ association is rapidly relieved at the DNA lesion site, to induce activation of the $CUL4A^{DDB2}$ complex. Thus, we examined the associations of both $CSN^{\Delta CSNAP}$ and the WT complex with $CUL4A^{DDB2}$ components, following the induction of DNA damage. Time-course analysis of DDB2 pull-downs from chromatin-bound fractions following UV irradiation indicated that, as expected, both DDB2 and DDB1 are rapidly recruited to chromatin (Fig. 4G). In WT cells,

we could detect CSN release from the DDB2 complex following UV irradiation. However, in ΔCSNAP cells, although release was observed after 20 minutes it was less significant and rapid restoration of CSN/DDB2 interaction was detected, compromising the activation of the DNA damage response through $CUL4A^{DDB2}$. This is observation is consistent with our in vitro binding data, which showed a stronger binding between Cul1/Rbx1 and $CSN^{\Delta CSNAP}$ versus CSN (Fig. 1E) and between CSN3 and DDB2 (Fig. 1B and C). Overall, these results support the view that the affinity of CSN for CRL complexes is enhanced, in the absence of CSNAP.

Discussion

Here, we investigated the functional contribution of CSNAP, the smallest and last to be discovered CSN subunit to the steric and catalytic functions of the CSN. We find that CSNAP attenuates CSN binding interactions with CRL (Fig. 5). Efficient dissociation from CRL assemblies is essential for reconfiguration of new CRL compositions in order to respond to changing regulatory inputs. Therefore, a hypothesis emerging from this study is that the increased affinity of $CSN^{\Delta CSNAP}$ for CRLs will affect the dynamic plasticity of CRL configuration. Indeed, we find that the absence of CSNAP alters cell cycle progression and reduces cellular viability. In addition, the impaired DNA damage response following UV irradiation of $CSN^{\Delta CSNAP}$ indicates a reduced capacity of ΔCSNAP cells to adapt to cellular stimuli. Together these results show that CSNAP contributes to the steric regulation of CRL by CSN, with global cellular effects.

Our data indicate that the K_d for CSN binding to Cul1 is at least 3 fold higher than for the complex lacking CSNAP (Fig. 1E). Given that the *Kd* is in the micromolar range, and that the cellular cullin and CSN concentrations are ~2.2 and 0.45 μM, respectively (Mosadeghi et al., 2016), the change in K_d would be expected to impact the free CSN and CRL pools. Unneddylated cullins bind Cand1 or Cand2, the F-box protein exchange factors that mediates CRL recycling (Liu et al., 2018, Pierce, Lee et al., 2013, Schmidt, McQuary et al., 2009) (Fig. 5). A portion of unneddylated cullins, however, were shown to remain unbound to Cand1 (Bennett, Rush et al., 2010, Liu, Zhou et al., 2017, Schmidt et al., 2009) and some SCF substrates are efficiently degraded independently of these exchange factors

(Liu et al., 2018, Scott & Schulman, 2018). Hence, free unneddylated cullins may be directly available for configuration of new CRL modules.

In line with this assumption, it was demonstrated recently that the presence of unneddylated Cul1 is important for maintaining the substrate receptor pool and promoting rapid assembly and activation of Cul1-Skp1-F-box complexes (Liu et al., 2017). Moreover, prolonging CSN-CRL interaction using irreversible neddylation inhibits CRL activity (Scherer, Ding et al., 2016). Likewise, strengthening the CRL-CSN interaction using the metabolite inositol hexakisphosphate promotes CRL inactivation (Scherer et al., 2016). Taken together with the present results, it is reasonable to conclude that modulation of CSN-CRL binding is an important mode of CRL regulation.

The recent crystal structure of free $CSN^{\Delta CSNAP}$ indicated that PCI and MPN subunits form largely distinct substructures (Lingaraju, Bunker et al., 2014). The six PCI subunits comprise the base of the CSN, with their C-terminal ends forming an elaborate bundle above which the heterodimer CSN5/CSN6 sits. Previously, we discovered that CSNAP tethers together these two distinct structural elements, by mutually binding CSN5/CSN6, and the PCI subunit CSN3. Both CSN5 and CSN3 directly interact with the CRL assembly, CSN3 with the substrate receptor (Cavadini, Fischer et al., 2016, Enchev et al., 2012), and CSN5 with the Nedd8 cullin modification (Cope et al., 2002). Thus, it is likely that through these interactions, CSNAP modulates CSN-CRL interactions. Unraveling the precise structural contribution of CSNAP to CSN-CRL binding affinity awaits high-resolution structural analyses; however, it is reasonable to speculate that CSNAP shifts the CSN conformational equilibrium toward low affinity states.

Given that CRLs are involved in regulating numerous cellular processes, including cell-division cycle and cellular proliferation, the correlation between aberrant CRL function and cancer is not surprising, making this system an attractive target for therapeutic intervention (reviewed in (Kitagawa & Kitagawa, 2016, Wang, Liu et al., 2014, Zhao & Sun, 2013)). For example Cul4/CRBN has been implicated as the target of the anti-myeloma agent lenalidomide (Lu, Middleton et al., 2014), and the neddylation inhibitor MLN4924 is an anti-cancer drug currently in clinical trials (Soucy et al., 2009). As a direct regulator of CRLs, the CSN constitutes another objective for drug development, with a

major focus on inhibiting CSN5, the catalytic subunit (Altmann, Erbel et al., 2017, Cope & Deshaies, 2006, Lauinger, Li et al., 2017, Lee, Judge et al., 2011, Pulvino, Chen et al., 2015, Schlierf, Altmann et al., 2016). Our latest findings lead us to propose CSNAP as a new therapeutic avenue. Preventing CSNAP integration within the CSN complex would be expected to impair cell cycle progression and the adaptive response to oncogenic stress conditions.

Materials and Methods

Cell cultures, transfections, and UV-C exposure

HAP1 WT and ΔCSNAP CRISPR cell lines were purchased from Haplogene GmbH, Austria, and cultured in a humidified CO_2 incubator at 37 °C in Iscove's Modified Dulbecco's Medium (IMDM) supplemented with 10% fetal calf serum, penicillin-streptomycin and Mycozap (Lonza). HAP1 cells were transfected with Hyg-CSNAP-Cerulean, Hyg-ΔN-CSNAP-Cerulean, or Hyg-FBXL15-FLAG, using the JetPrime reagent (Polyplus). Cerulean-expressing cell lines were isolated and sorted for low-medium expression levels by fluorescence-activated cell sorting (FACSAria Fusion; BD Biosciences), and expanded in complete IMDM. For UV treatments, plates were washed twice with PBS, and after removal of the liquid, were illuminated with 5 or 20J/m^2 UV-C light.

Immunoprecipitation and FLAG-pull down

For immunoprecipitation experiments, HAP1 cells were lysed in 50 mM Tris pH 7.4, 150 mM NaCl, 0.5% NP40, phosphatase inhibitors (5 mM Na-o-vanadate, 4 mM Na-pyrophosphate and β-glycerophosphate) and protease inhibitors inhibitors (1 mM PMSF, 1 mM benzamidine, 1.4 μg/ml pepstatin A. 0.25-1 mg total protein was incubated with 10μl anti-CSN3 (Abcam ab79398), anti-DDB2 (Santa Cruz sc-81246) or 35μl anti-FLAG resin (Sigma A2220) overnight. For immunoprecipitation of the CSN3 or DDB2 antibody 35μl protein G sepharose slurry was added for 1 hour. Bound proteins were washed and eluted with 2x Laemmli sample buffer. Chromatin-bound proteins were purified as previously described (Fuzesi-Levi et al., 2014), using 50 μg/ml digitonin instead of NP40 in the hypotonic lysis buffer. 250 μg of chromatin bound fraction was suspended in 250 μl TBS and rotated overnight at 4 ºC with 5 μl of anti-DDB2 (Santa Cruz sc-81246). Then 30

µl of TBS equilibrated Protein G Sepharose resin (GE) was added for 1 hour, and after 3 washes of 300 µl TBS bound proteins were eluted in 35 µl 2x Laemmli sample buffer.

Fluorescence assays

Purification of recombinant $CSN^{\Delta CSNAP}$ complexes was performed as described in (Enchev et al., 2012). The production of CSN and CSN^{5H138A} involved the generation of a pFBDM vector containing CSN1/His6-CSN5/CSN2/StrepII2x-CSN3/CSNAP or CSN1/His6-$CSN5^{H138A}$/CSN2/StrepII2x-CSN3/CSNAP respectively. Baculoviruses produced from each of these vectors were used to co-infect HighFive insect cells with a baculovirus expressing CSN4/CSN7b/CSN6/CSN8 to produce the full complexes. The fluorescent assays to determine the affinity of the CSN complexes for Cul1-dansyl/Rbx1 variants and their deneddylation activity were performed as described in (Mosadeghi et al., 2016).

Western blots

Proteins were separated on 12% SDS-PAGE, and transferred to PVDF membranes. Primary antibodies used for detection: anti-CSN1 (Enzo PW8285), anti-CSN2 (Abcam ab10462), anti-CSN3 (ab79398), anti-CSN5 (ab495 and ab118841), anti-CSN6 (PW 8295), anti-CSN8 (BML-PW8290), anti-PDCD4 (ab80590), anti-cullin1 (ab75817), anti-cullin2 (ab166917), anti-cullin3 (ab75851), anti-cullin4AB (ab76470), anti-cullin5 (ab184177), anti-DDB1 (Bethyl A300-462A), anti-DDB2 (ab181136), anti-PARP1 (sc-8007), anti-FLAG (Sigma F3165), anti-pChk1 (Cell signaling 2341), anti-GAPDH (Millipore MAB374), anti-vimentin (ab92547), anti-NQO1 (ab28947), anti-tubulin (ab184613), and anti-histone 3 (ab24834). All Western blot analyzes were repeated at least three times.

Comet assay

Alkaline single-cell electrophoresis was performed, according to the protocol from Trevigen. HAP1 cells were treated with $20J/m^2$ UV-C light, and 6 hours post-exposure cells were trypsinized, counted, and suspended in ice-cold PBS (-Ca/-Mg) to a density of $2x10^5$ cells/ml. Fifty µl of cell suspension were mixed with 450 µl LM-agarose (Trevigen), and 50 µl of the mix was pipetted onto the comet slide, and incubated in the dark at 4 °C for 30 minutes. Slides were immersed in a lysis solution (Trevigen) for 1 hour at 4 °C, and then equilibrated to an alkaline electrophoresis solution (300 mM NaOH, 2 mM EDTA,

pH>13) for 20 minutes at room temperature. Slides were run at 1 V/cm (~300 mA constant) in ice-cold alkaline electrophoresis solution for 30 minutes and then neutralized for 5 minutes in 400 mM Tris, pH7.5, rinsed in distilled water, immersed in 70% ethanol for 5 minutes and dried at room temperature. DNA was stained with SYBR Gold (Invitrogen); the slides were then dried completely, prior to imaging. Images were acquired using an inverted Nikon microscope (Eclipse Ti, Nikon, Japan) using a 20x objective, and with a cooled electron-multiplying charge-coupled device camera (iXon Ultra, Andor, Ireland). Comet parameters were analyzed using the CASP comet software. At least 74 cells were analyzed per sample, in 3 biological samples, in duplicates.

Colony-forming assay

Untreated or 20J/m^2 UV-C exposed WT and ΔCSNAP cells were trypsinized, counted, and plated in 10 cm tissue culture dishes in triplicates. For untreated cells, 100 cells, and for UV-illuminated cells, 5,000 cells were plated per dish. All experiments were done in triplicates. Dishes were incubated in normal growth conditions for 8 days. The plates were then washed twice with PBS, dried, and stained with 0.15% Crystal violet in methanol for 3 minutes, rinsed with tap water, and air-dried before scanning. Colony counts were measured using OpenCFU software.

Cell cycle analysis

Cells were synchronized to G1/S phase using double thymidine block as previously described (Fuzesi-Levi et al., 2014). UV treated cells were exposed to 5 J/m^2 UV-C at release, and fixed with ethanol at different time points. Cell cycle phases were assessed by flow cytometry (LSRII, BD Biosciences) following propidium iodide staining. Asynchronous cells were analyzed using propidium iodide and BrdU double staining. 10^5 cells were denatured after fixation using 2N HCl, 0.5% Triton X-100 in PBS for 30 minutes, neutralized in 0.1 M $Na_2B_4O_7$ pH 8.5 and incubated with 5 µl of anti-BrdU-FITC (eBioscience 11-5071-41) in 1% BSA, 0.5% Triton X-100 in PBS for 1 hour. Cells were washed in 1% BSA in PBS, resuspended in PBS containing 50 µg/ml propidium iodide and 50 µg/ml RNase A, and analysed in FACSAria Fusion flow cytometer (BD Biosciences).

Measurement of viable and dead cell populations

Determination of percentage of live, early apoptotic and late apoptotic/necrotic cells in WT and ΔCSNAP cultures was performed using Annexin V-FITC Apoptosis Detection Kit (APOAF-20TST, Sigma) by flow cytometry. Single cells were analyzed for AnnexinV-FITC and propidium iodide fluorescence. Early apoptotic cells (annexin V positive, PI negative), late apoptotic/necrotic/dead cells (annexin V positive, PI positive), and live/viable cells (annexin V negative, PI negative) were gated and quantified.

Resazurin assay

WT, ΔCSNAP, ΔCSNAP-Cerulean and ΔCSNAP-ΔC-Cerulean expressing cells were trypsinized, counted, and seeded in 4 replicates at a cell density of 5000 cells/well in 24 well plates. Cells in one plate were seeded directly to 30 μg/ml resazurin containing growth medium, and fluourescence intensity (540/600nm) was measured after 2 hours, for initial proliferation value. The other plates were either UV-exposed at 20 J/m^2 24 hours after seeding or left untreated. Two or 4 hours post-UV the growth medium was changed to 30 μg/ml resazurin containing medium, incubated for 2 hours, and fluorescence was measured. Proliferation was calculated at each time point normalizing to the initial proliferation value.

SILAC

HAP1 cells were grown in SILAC IMDM (Invitrogen) with 10% dialyzed fetal calf serum (Biological Industries, 04-011-1A) supplemented with 2 5 μg/ml light L-lysine and L-arginine (Sigma) or 25 μg/ml heavy L-lysine (L-Lys8- CNLM-291-H-1, Cambridge Isotopes) and L-arginine (L-Arg10-CNLM-539-H-1, Cambridge Isotopes) each, and labeling was swapped between WT and ΔCSNAP cells. Cells were incubated with 5μM MG132 for 4 hours before harvesting. Samples were prepared, as previously described (Udeshi, Svinkina et al., 2013). Briefly, the samples were lysed using 8 M urea, mixed at a 1:1 protein:protein ratio, and digested with trypsin, followed by a desalting step. The resulting peptides were fractionated offline using high pH-reversed phase chromatography, followed by enrichment for K-ε-GlyGly using the Cell Signaling PTMScan® Ubiquitin Remnant Motif (K-ε-GG) Kit #5562 (antibody- based). Each fraction was then analyzed, using online nanoflow liquid chromatography (nanoAcquity) coupled to high-resolution,

high-mass accuracy mass spectrometry (Fusion Lumos). Raw data was processed with MaxQuant v1.5.5.1. The data was searched with the Andromeda search engine against the human proteome database appended with common lab protein contaminants, and allowing for GG modifications of lysines. The ratio of H/L (heavy to light) ratio was calculated, and results were log-transformed. The datasets of four (two label swap) experiments were combined in the way, that the experiment with the largest number of proteins identified was merged with proteins that had data for the same proteins and modification sites from the three other experiments. Genes corresponding to proteins that showed fold change above 1.5 or below 0.66 in each of the four experiments were filtered, and were selected only if appeared at least two out of the four experiments (from non-unique proteins only the first in the gene list was included). The resulting protein/gene list from was analyzed using EnrichR/Reactome 2016 or Webgestalt/Reactome 2016 for overrepresentation, and results were filtered using a cut off of adjusted p value or FDR < 0.05.

Label-free quantitation

WT and ΔCSNAP cells were lysed in 50 mM Tris, pH 7.4, 150 mM NaCl, 0.5% NP40, supplemented with phosphatase and protease inhibitors as described above. One mg total protein was used for immunoprecipitation, using anti-CSN3 antibody (ab79698) as described above in 3 biological replicates. Proteins were eluted by 75 µl of 0.1 M glycine-HCl, pH 2.5. The beads were washed in 25 mM Tris pH7.4, 150 mM NaCl (TBS), and subjected to on-bead tryptic digestion as follows: 8 M urea in 0.1 M Tris, pH 7.9, was added onto TBS washed beads, and incubated for 15 minutes at room temperature. Proteins were reduced by incubation with dithiothreitol (5 mM; Sigma) for 60 minutes at room temperature, and alkylated with 10 mM iodoacetamide (Sigma) in the dark for 30 minutes at room temperature. Urea was diluted to 2M with 50mM ammonium bicarbonate. Trypsin (250 ng; Promega; Madison, WI, USA) was added and incubated overnight at 37 °C, followed by addition of 100 ng trypsin for 4 hour at 37 °C. Digestions were stopped by addition of trifluoroacetic acid (1% final concentration). Following digestion, peptides were desalted using Oasis HLB µElution format (Waters, Milford, MA, USA), vacuum-dried, and stored at -80˚C until further analysis.

ULC/MS grade solvents were used for all chromatographic steps. Each sample was loaded using split-less nano-Ultra Performance Liquid Chromatography (10 kpsi nanoAcquity; Waters). The mobile phase was: A) H_2O + 0.1% formic acid and B) acetonitrile + 0.1% formic acid. Sample desalting was performed online, using a reversed-phase Symmetry C_{18} trapping column (180 µm internal diameter, 20 mm length, 5 µm particle size; Waters). The peptides were then separated using a T3 HSS nano-column (75 µm internal diameter, 250 mm length, 1.8 µm particle size; Waters) at 0.35 µL/min. Peptides were eluted from the column into the mass spectrometer, using the following gradient: 4% to 30% B for 55 min, 30% to 90% B for 5 min, maintained at 90% for 5 min, and then back to initial conditions. The nanoUPLC was coupled online through a nanoESI emitter (10 µm tip; New Objective; Woburn, MA, USA) to a quadrupole orbitrap mass spectrometer (Q Exactive Plus, Thermo Scientific), using a FlexIon nanospray apparatus (Proxeon).

Data was acquired in data-dependent acquisition (DDA) mode, using a Top20 method. MS1 resolution was set to 70,000 (at 400 m/z), mass range of 300-1650 m/z, AGC of 3e6, and maximum injection time was set to 20 msec. MS2 resolution was set to 17,500, quadrupole isolation 1.7 m/z, AGC of 1e6, dynamic exclusion of 30 sec, and maximum injection time of 60 msec. Raw data was imported into Expressionist® software version 9.1.3 (Genedata), and processed as described here. The software was used for retention time alignment and peak detection of precursor peptides. A master peak list was generated from all MS/MS events, and sent for database searching using Mascot v2.5.1 (Matrix Sciences). Data was searched against the human sequences UniprotKB (http://www.uniprot.org/), appended with the CSNAP sequence and common laboratory contaminant proteins. Fixed modification was set to carbamidomethylation of cysteines, and variable modifications were set to oxidation of methionines and deamidation of N or Q. Search results were then filtered using the PeptideProphet algorithm, to achieve a maximum false discovery rate of 1% at the protein level. Peptide identifications were imported back to Expressionist to annotate identified peaks. Quantification of proteins from the peptide data was performed, using an in-house script. Data was normalized, based on the total ion current. Protein abundance was obtained by summing the three most intense, unique peptides per protein. A Student's t-test, after logarithmic transformation, was used to identify significant differences (>1.5-fold) across the biological replica. Fold

changes were calculated based on the ratio of arithmetic means of the case versus control samples.

Total proteome analysis and bioinformatics

WT and ΔCSNAP cells were lysed in SDT buffer (4% SDS, 100 mM Tris/HCl, pH 7.6, and 0.1 M dithiothreitol) and subjected to tryptic digestion, using a FASP™ Protein Digestion Kit (Expedeon). The resulting peptides were desalted and analyzed on the LC-MS instrument (Q-Exactive Plus) in DDA mode. The raw data was processed in Expressionist by Genedata, using Mascot as the search engine against the uniprot human proteome database, and common protein contaminants. Identifications were filtered to a maximum of 1% FDR on both the peptide and protein levels. Protein inference was performed by an in-house script. Overall, about 4,000 proteins were identified and quantified. Proteomics data, after logarithmic transformation and flooring, were analyzed by two-way ANOVA using two factors, strain and UV treatment, as well as their interaction. Proteins with a p value of <0.05 and an absolute fold change >1.5 were considered to be differentially expressed. The proteins were filtered to keep those that had an absolute fold change of at least 1.5 and a p-value of <0.05 in at least one of the following pairwise comparisons: 1. WT UV/WT untreated; 2. ΔCSNAP UV/ ΔCSNAP untreated; 3. ΔCSNAP untreated/ WT untreated; 4. ΔCSNAP UV/ WT UV. The log intensities of the 347 proteins that passed these criteria (according to ANOVA analysis with all samples, after flooring was used). Intensities were clustered using the k-means algorithm, with Pearson dissimilarity as the distance measure to 5 clusters. Log_2 intensities were standardized, so that each protein displayed zero mean and unit standard deviation. The proteins in each cluster could be obtained by filtering the Excel file. Enrichment analysis of the filtered protein list was performed using Webgestalt overrepresentation analysis using Reactome 2016 pathway as functional database against the protein coding database as reference set, and results were filtered for adjusted p value <0.05.

All raw data, peak lists and identifications were deposited to the ProteomeXchange Consortium http://proteomecentral.proteomexchange.org) via the PRIDE partner repository.

Native mass spectrometry

Nano-electrospray ionization mass spectrometry (MS) experiments were performed on a modified Q Exactive Plus Orbitrap EMR (Ben-Nissan, Belov et al., 2017). Prior to MS analysis, 25 µl of the samples (~ 16 µM) were buffer-exchanged into 0.5 M ammonium acetate (pH 7), using Bio-Rad Biospin columns. Two µl of the buffer-exchanged samples were mixed with 1 µl MeOH 40%, to reach a final concentration of 13%. Proteins were loaded into gold coated nano-ESI capillaries, prepared in house from borosilicate glass tubes (Kirshenbaum, Michaelevski et al., 2010). For the reconstitution of the CSN complex, after buffer exchange, 2 µl of $CSN^{\Delta CSNAP}$, were incubated for 3 h on ice with 2 µl of a synthetic CSNAP peptide, dissolved to 50 µM in 250 mM ammonium acetate. The conditions within the mass spectrometer were adjusted to optimize signals of the intact CSN and preserve non-covalent interactions. The instrument was operated in positive mode at capillary voltage of 1.7 kV. Argon was used as the collision gas in the higher energy collision-induced dissociation (HCD) cell. Resolution was set to 8750. Forevacuum was set to 1.5 mbar and the trapping gas was set to 3, corresponding to pressures of 8.8x10-5 and 1.7x10-10 mbar in the HV and UHV regions, respectively. Flatapole bias was set to transmission at 1.5 V. Bent flatapole and axial gradient were set to DC 2.2 V and 37.2 V, respectively. HCD cell bias was set to 150 V. Spectra are shown with no smoothing and without background subtraction.

Acknowledgments

We thank Dieter A. Wolf for comments on the manuscript, and Dr. Ron Rotkopf for the statistical analysis. M.S. is grateful for the financial support of the US National Institutes of Health, grant no. GM121834. M.S. is the incumbent of the Aharon and Ephraim Katzir Memorial Professorial Chair. G.F. is the Incumbent of the David and Stacey Cynamon Research fellow Chair in Genetics and Personalized Medicine

Author contribution

M.G.F.-L., G.B-N., R.I.E., M.P. and M.S. designed the experiments and analyzed the data. M.G.F.-L. performed the cell biology and biochemistry experiments. M.G.F.-L and T.M.S performed the flow cytometry, and M.G.F.-L., and R.N. performed the microscopy

experiments. G.B-N. performed the mass spectrometry and R.I.E. the K_d measurement experiments. Y.L. and M.K. performed the SILAC and label-free proteomics analysis. G.F. performed the bioinformatics analysis of the proteomics data. M.G.F.-L, G.B.-N., and M.S. wrote the manuscript.

Conflict of interest

The authors have no conflict of interest

References

Altmann E, Erbel P, Renatus M, Schaefer M, Schlierf A, Druet A, Kieffer L, Sorge M, Pfister K, Hassiepen U, Jones M, Ruedisser S, Ostermeier D, Martoglio B, Jefferson AB, Quancard J (2017) Azaindoles as zinc-binding small-molecule inhibitors of the JAMM Protease CSN5. *Angewandte Chemie* 56: 1294-1297

Ben-Nissan G, Belov ME, Morgenstern D, Levin Y, Dym O, Arkind G, Lipson C, Makarov AA, Sharon M (2017) Triple-Stage Mass Spectrometry Unravels the Heterogeneity of an Endogenous Protein Complex. *Analytical chemistry* 89: 4708-4715

Bennett EJ, Rush J, Gygi SP, Harper JW (2010) Dynamics of cullin-RING ubiquitin ligase network revealed by systematic quantitative proteomics. *Cell* 143: 951-65

Cavadini S, Fischer ES, Bunker RD, Potenza A, Lingaraju GM, Goldie KN, Mohamed WI, Faty M, Petzold G, Beckwith RE, Tichkule RB, Hassiepen U, Abdulrahman W, Pantelic RS, Matsumoto S, Sugasawa K, Stahlberg H, Thoma NH (2016) Cullin-RING ubiquitin E3 ligase regulation by the COP9 signalosome. *Nature* 531: 598-603

Chaitanya GV, Steven AJ, Babu PP (2010) PARP-1 cleavage fragments: signatures of cell-death proteases in neurodegeneration. *Cell Commun Signal* 8: 31

Cope GA, Deshaies RJ (2006) Targeted silencing of Jab1/Csn5 in human cells downregulates SCF activity through reduction of F-box protein levels. *BMC Biochem* 7: 1

Cope GA, Suh GS, Aravind L, Schwarz SE, Zipursky SL, Koonin EV, Deshaies RJ (2002) Role of predicted metalloprotease motif of Jab1/Csn5 in cleavage of Nedd8 from Cul1. *Science* 298: 608-11

Deshaies RJ, Joazeiro CA (2009) RING domain E3 ubiquitin ligases. *Annual review of biochemistry* 78: 399-434

Dubois EL, Gerber S, Kisselev A, Harel-Bellan A, Groisman R (2016) UV-dependent phosphorylation of COP9/signalosome in UV-induced apoptosis. *Oncol Rep* 35: 3101-5

Emanuele MJ, Elia AE, Xu Q, Thoma CR, Izhar L, Leng Y, Guo A, Chen YN, Rush J, Hsu PW, Yen HC, Elledge SJ (2011) Global identification of modular cullin-RING ligase substrates. *Cell* 147: 459-74

Emberley ED, Mosadeghi R, Deshaies RJ (2012) Deconjugation of Nedd8 from Cul1 is directly regulated by Skp1-F-box and substrate, and the COP9 signalosome inhibits deneddylated SCF by a noncatalytic mechanism. *The Journal of biological chemistry* 287: 29679-89

Enchev RI, Schulman BA, Peter M (2015) Protein neddylation: beyond cullin-RING ligases. *Nature reviews Molecular cell biology* 16: 30-44

Enchev RI, Scott DC, da Fonseca PC, Schreiber A, Monda JK, Schulman BA, Peter M, Morris EP (2012) Structural basis for a reciprocal regulation between SCF and CSN. *Cell reports* 2: 616-27

Fischer ES, Scrima A, Bohm K, Matsumoto S, Lingaraju GM, Faty M, Yasuda T, Cavadini S, Wakasugi M, Hanaoka F, Iwai S, Gut H, Sugasawa K, Thoma NH (2011) The molecular basis of CRL4DDB2/CSA ubiquitin ligase architecture, targeting, and activation. *Cell* 147: 1024-39

Franken NA, Rodermond HM, Stap J, Haveman J, van Bree C (2006) Clonogenic assay of cells in vitro. *Nat Protoc* 1: 2315-9

Fuzesi-Levi MG, Ben-Nissan G, Bianchi E, Zhou H, Deery MJ, Lilley KS, Levin Y, Sharon M (2014) Dynamic regulation of the COP9 signalosome in response to DNA damage. *Molecular and cellular biology* 34: 1066-76

Gentile M, Latonen L, Laiho M (2003) Cell cycle arrest and apoptosis provoked by UV radiation-induced DNA damage are transcriptionally highly divergent responses. *Nucleic Acids Res* 31: 4779-90

Glickman MH, Rubin DM, Coux O, Wefes I, Pfeifer G, Cjeka Z, Baumeister W, Fried VA, Finley D (1998) A subcomplex of the proteasome regulatory particle required for ubiquitin-conjugate degradation and related to the COP9-signalosome and eIF3. *Cell* 94: 615-23

Groisman R, Polanowska J, Kuraoka I, Sawada J, Saijo M, Drapkin R, Kisselev AF, Tanaka K, Nakatani Y (2003) The ubiquitin ligase activity in the DDB2 and CSA complexes is differentially regulated by the COP9 signalosome in response to DNA damage. *Cell* 113: 357-67

Hannss R, Dubiel W (2011) COP9 signalosome function in the DDR. *FEBS letters* 585: 2845-52

Hershko A, Ciechanover A, Varshavsky A (2000) Basic Medical Research Award. The ubiquitin system. *Nature medicine* 6: 1073-81

Hofmann K, Bucher P (1998) The PCI domain: a common theme in three multiprotein complexes. *Trends in biochemical sciences* 23: 204-5

Kaufmann SH, Desnoyers S, Ottaviano Y, Davidson NE, Poirier GG (1993) Specific proteolytic cleavage of poly(ADP-ribose) polymerase: an early marker of chemotherapy-induced apoptosis. *Cancer research* 53: 3976-85

Kirshenbaum N, Michaelevski I, Sharon M (2010) Analyzing large protein complexes by structural mass spectrometry. *Journal of visualized experiments : JoVE*

Kitagawa K, Kitagawa M (2016) The SCF-type E3 ubiquitin ligases as cancer targets. *Curr Cancer Drug Targets* 16: 119-29

Koren I, Timms RT, Kula T, Xu Q, Li MZ, Elledge SJ (2018) The Eukaryotic Proteome Is Shaped by E3 Ubiquitin Ligases Targeting C-Terminal Degrons. *Cell* 173: 1622-1635 e14

Lauinger L, Li J, Shostak A, Cemel IA, Ha N, Zhang Y, Merkl PE, Obermeyer S, Stankovic-Valentin N, Schafmeier T, Wever WJ, Bowers AA, Carter KP, Palmer AE, Tschochner H, Melchior F, Deshaies RJ, Brunner M, Diernfellner A (2017) Thiolutin is a zinc chelator that inhibits the Rpn11 and other JAMM metalloproteases. *Nat Chem Biol* 13: 709-714

Lee YH, Judge AD, Seo D, Kitade M, Gomez-Quiroz LE, Ishikawa T, Andersen JB, Kim BK, Marquardt JU, Raggi C, Avital I, Conner EA, MacLachlan I, Factor VM, Thorgeirsson SS (2011) Molecular targeting of CSN5 in human hepatocellular carcinoma: a mechanism of therapeutic response. *Oncogene* 30: 4175-84

Lingaraju GM, Bunker RD, Cavadini S, Hess D, Hassiepen U, Renatus M, Fischer ES, Thoma NH (2014) Crystal structure of the human COP9 signalosome. *Nature* 512: 161-5

Liu Q, Zhou Y, Tang R, Wang X, Hu Q, Wang Y, He Q (2017) Increasing the unneddylated Cullin1 portion rescues the CSN phenotypes by stabilizing adaptor modules to drive SCF assembly. *Molecular and cellular biology* 37: e00109-17

Liu X, Reitsma JM, Mamrosh JL, Zhang Y, Straube R, Deshaies RJ (2018) Cand1-mediated adaptive exchange mechanism enables variation in F-Box protein expression. *Molecular cell* 69: 773-786 e6

Lu G, Middleton RE, Sun H, Naniong M, Ott CJ, Mitsiades CS, Wong KK, Bradner JE, Kaelin WG, Jr. (2014) The myeloma drug lenalidomide promotes the cereblon-dependent destruction of Ikaros proteins. *Science* 343: 305-9

Meir M, Galanty Y, Kashani L, Blank M, Khosravi R, Fernandez-Avila MJ, Cruz-Garcia A, Star A, Shochot L, Thomas Y, Garrett LJ, Chamovitz DA, Bodine DM, Kurz T, Huertas P, Ziv Y, Shiloh Y (2015) The COP9 signalosome is vital for timely repair of DNA double-strand breaks. *Nucleic acids research* 43: 4517-30

Mosadeghi R, Reichermeier KM, Winkler M, Schreiber A, Reitsma JM, Zhang Y, Stengel F, Cao J, Kim M, Sweredoski MJ, Hess S, Leitner A, Aebersold R, Peter M, Deshaies RJ, Enchev RI (2016) Structural and kinetic analysis of the COP9-Signalosome activation and the cullin-RING ubiquitin ligase deneddylation cycle. *Elife* 5

Olive PL, Banath JP (2006) The comet assay: a method to measure DNA damage in individual cells. *Nat Protoc* 1: 23-9

Ong SE, Blagoev B, Kratchmarova I, Kristensen DB, Steen H, Pandey A, Mann M (2002) Stable isotope labeling by amino acids in cell culture, SILAC, as a simple and accurate approach to expression proteomics. *Molecular & cellular proteomics : MCP* 1: 376-86

Pierce NW, Lee JE, Liu X, Sweredoski MJ, Graham RL, Larimore EA, Rome M, Zheng N, Clurman BE, Hess S, Shan SO, Deshaies RJ (2013) Cand1 promotes assembly of new SCF complexes through dynamic exchange of F box proteins. *Cell* 153: 206-15

Pulvino M, Chen L, Oleksyn D, Li J, Compitello G, Rossi R, Spence S, Balakrishnan V, Jordan C, Poligone B, Casulo C, Burack R, Shapiro JL, Bernstein S, Friedberg JW, Deshaies RJ, Land H, Zhao J (2015) Inhibition of COP9-signalosome (CSN) deneddylating activity and tumor growth of diffuse large B-cell lymphomas by doxycycline. *Oncotarget* 6: 14796-813

Reitsma JM, Liu X, Reichermeier KM, Moradian A, Sweredoski MJ, Hess S, Deshaies RJ (2017) Composition and Regulation of the Cellular Repertoire of SCF Ubiquitin Ligases. *Cell* 171: 1326-1339 e14

Rozen S, Fuzesi-Levi MG, Ben-Nissan G, Mizrachi L, Gabashvili A, Levin Y, Ben-Dor S, Eisenstein M, Sharon M (2015) CSNAP Is a stoichiometric subunit of the COP9 signalosome. *Cell Rep* 13: 585-98

Scherer PC, Ding Y, Liu Z, Xu J, Mao H, Barrow JC, Wei N, Zheng N, Snyder SH, Rao F (2016) Inositol hexakisphosphate (IP6) generated by IP5K mediates cullin-COP9 signalosome interactions and CRL function. *Proceedings of the National Academy of Sciences of the United States of America* 113: 3503-8

Schlierf A, Altmann E, Quancard J, Jefferson AB, Assenberg R, Renatus M, Jones M, Hassiepen U, Schaefer M, Kiffe M, Weiss A, Wiesmann C, Sedrani R, Eder J, Martoglio B (2016) Targeted inhibition of the COP9 signalosome for treatment of cancer. *Nature communications* 7: 13166

Schmidt MW, McQuary PR, Wee S, Hofmann K, Wolf DA (2009) F-box-directed CRL complex assembly and regulation by the CSN and CAND1. *Molecular cell* 35: 586-97

Scott DC, Schulman BA (2018) SCF E3 ligase substrates switch from CAN-D to can-ubiquitylate. *Molecular cell* 69: 721-723

Shalit T, Elinger D, Savidor A, Gabashvili A, Levin Y (2015) MS1-based label-free proteomics using a quadrupole orbitrap mass spectrometer. *Journal of proteome research* 14: 1979-86

Skaar JR, Pagan JK, Pagano M (2013) Mechanisms and function of substrate recruitment by F-box proteins. *Nature reviews Molecular cell biology* 14: 369-81

Soldani C, Scovassi AI (2002) Poly(ADP-ribose) polymerase-1 cleavage during apoptosis: an update. *Apoptosis* 7: 321-8

Soucy TA, Smith PG, Milhollen MA, Berger AJ, Gavin JM, Adhikari S, Brownell JE, Burke KE, Cardin DP, Critchley S, Cullis CA, Doucette A, Garnsey JJ, Gaulin JL, Gershman RE, Lublinsky AR, McDonald A, Mizutani H, Narayanan U, Olhava EJ et al. (2009) An inhibitor of NEDD8-activating enzyme as a new approach to treat cancer. *Nature* 458: 732-6

Udeshi ND, Mertins P, Svinkina T, Carr SA (2013) Large-scale identification of ubiquitination sites by mass spectrometry. *Nat Protoc* 8: 1950-60

Udeshi ND, Svinkina T, Mertins P, Kuhn E, Mani DR, Qiao JW, Carr SA (2013) Refined preparation and use of anti-diglycine remnant (K-epsilon-GG) antibody enables routine quantification of 10,000s of ubiquitination sites in single proteomics experiments. *Molecular & cellular proteomics : MCP* 12: 825-31

Wang Z, Liu P, Inuzuka H, Wei W (2014) Roles of F-box proteins in cancer. *Nature reviews Cancer* 14: 233-47

Wei N, Deng XW (2003) The COP9 signalosome. *Annu Rev Cell Dev Biol* 19: 261-86

Wei N, Serino G, Deng XW (2008) The COP9 signalosome: more than a protease. *Trends in biochemical sciences* 33: 592-600

Yen HC, Elledge SJ (2008) Identification of SCF ubiquitin ligase substrates by global protein stability profiling. *Science* 322: 923-9

Zhao Y, Sun Y (2013) Cullin-RING ligases as attractive anti-cancer targets. *Curr Pharm Des* 19: 3215-25

Zheng N, Zhou Q, Wang Z, Wei W (2016) Recent advances in SCF ubiquitin ligase complex: Clinical implications. *Biochimica et biophysica acta* 1866: 12-22

Figures

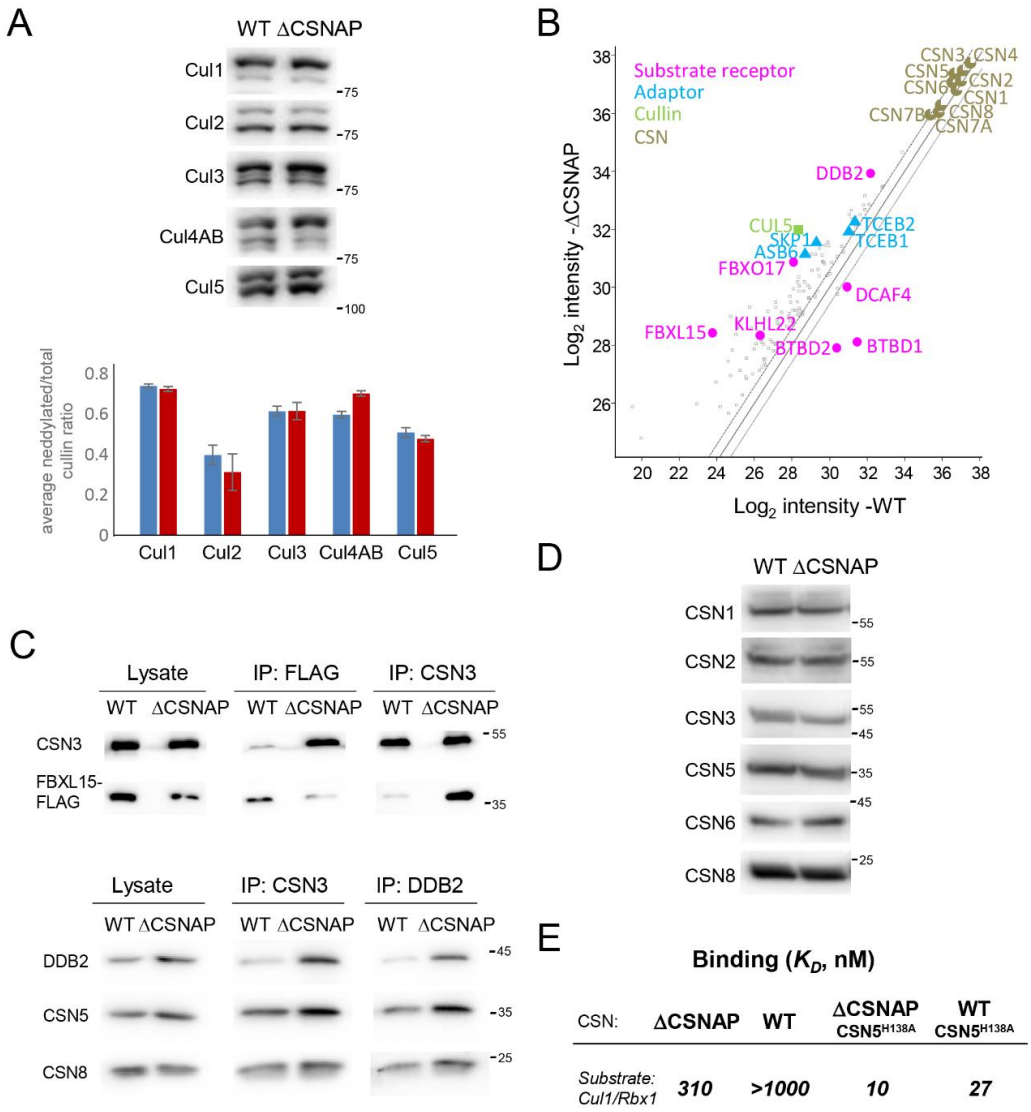

Figure 1. CSNAP modifies the strength of CSN-CRL interactions.

(A) CSN catalytic activity is not significantly affected by the absence of CSNAP. A representative western blot of WT and ΔCSNAP cell extracts visualized using antibodies against various cullins (top) and a plot demonstrating the average deneddylated fraction. The graph represents the averages of three independent experiments, with standard errors.

(B) CSN and its interacting proteins were pulled down using an antibody against CSN3 from WT and ΔCSNAP cells. Immunoprecipitated proteins were then analyzed by label-free proteomics approach using three biological replicates. Scatter plot comparing $\log_2$ intensities of proteins in ΔCSNAP and WT samples show that a number of CRL proteins were found to be over- or underrepresented in the pulldown of the CSN and $CSN^{\Delta CSNAP}$ complexes. In contrast, the ratio of average intensities for CSN subunits did not exceed the fold change of ΔCSNAP/WT > 1.5, which was considered to be the cut-off for fold change.

(C) Validation of the proteomics data for FBXL15/CSN and DDB2/CSN interactions. Reciprocal immunoprecipitation shows a tighter CSN3 interaction with FBXL15 and DDB2, in the absence of CSNAP.

(D) The levels of CSN subunits are comparable in WT and ΔCSNAP cells; thus, the differences in the amount of the pulled-down proteins are likely due to different interaction affinities. Representative blot out of three repeats.

(E) Determination of the dissociation constant (K_d) for the CSN and $CSN^{\Delta CSNAP}$ complexes, and dansyl-labeled Cul1-N8/Rbx1. The absence of CSNAP causes tighter binding to cullin1/Rbx1.

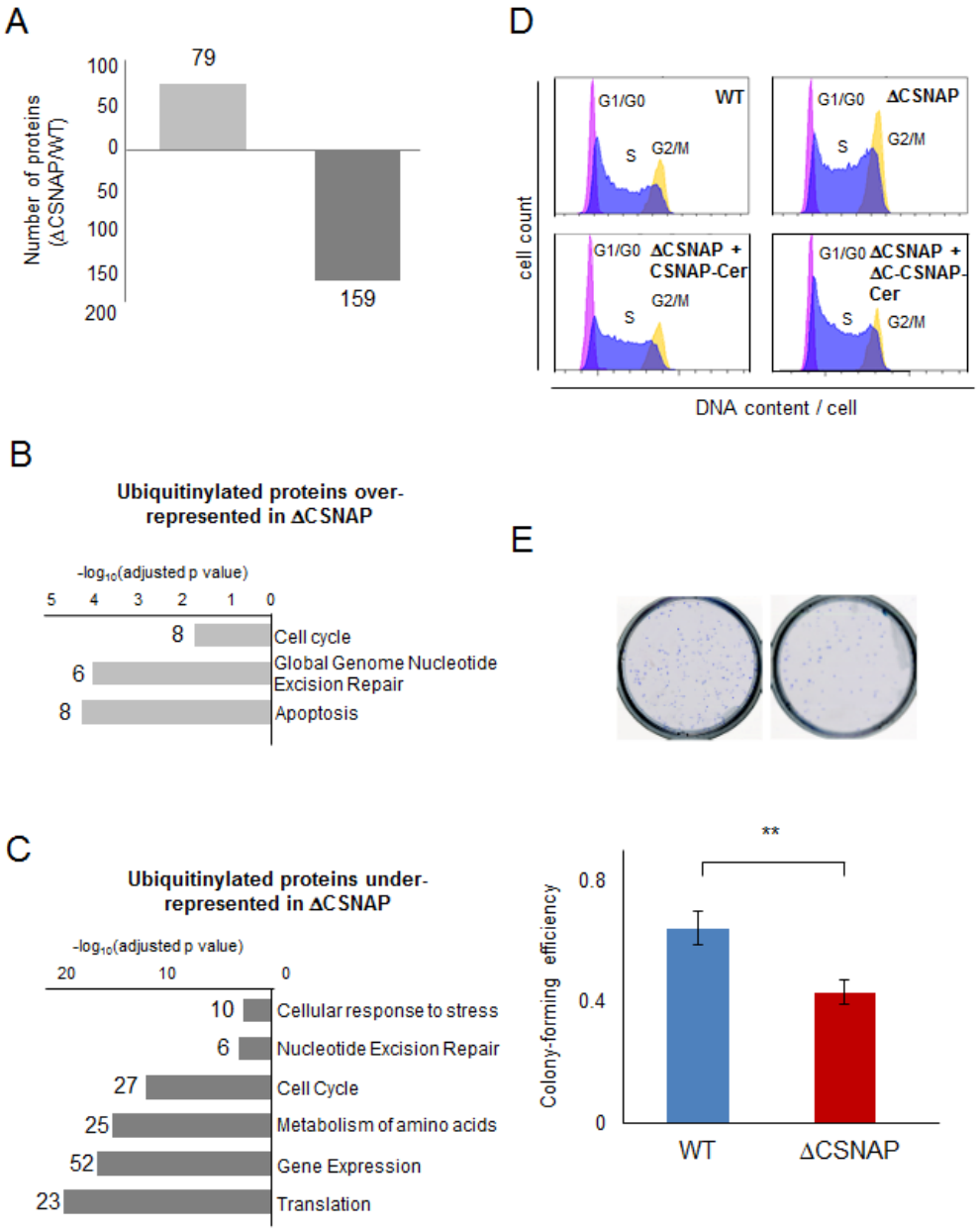

Figure 2. The absence of CSNAP impairs cell cycle progression and viability.

(A) We monitored protein ubiquitinylation in stable heavy and light isotope labelled ΔCSNAP and WT cells. The bar plot shows the number of differentially ubiquitinated (up or down) proteins that appeared in at least two out of four independent experiments.

(B-C) Pathway analysis of the proteins that are differentially ubiqiutinylated in ΔCSNAP and WT cells.

(D) Validation of the influence of the absence of CSNAP on cell cycle. Histograms of BrdU and propidium iodide stained asynchronous cells show that the lack of CSNAP results in a S-G2 shifted phenotype, that can be rescued by the expression of CSNAP-Cerulean, but not when its C-terminal CSN interacting domain is absent. The figure shows a representative experiment out of three.

(E) Cells lacking CSNAP have lower colony forming potential than WT cells. The graph represents the results from 14 biological replicates, significance was calculated using Student's t-test (** $p<0.001$). Images above show a representative experiment.

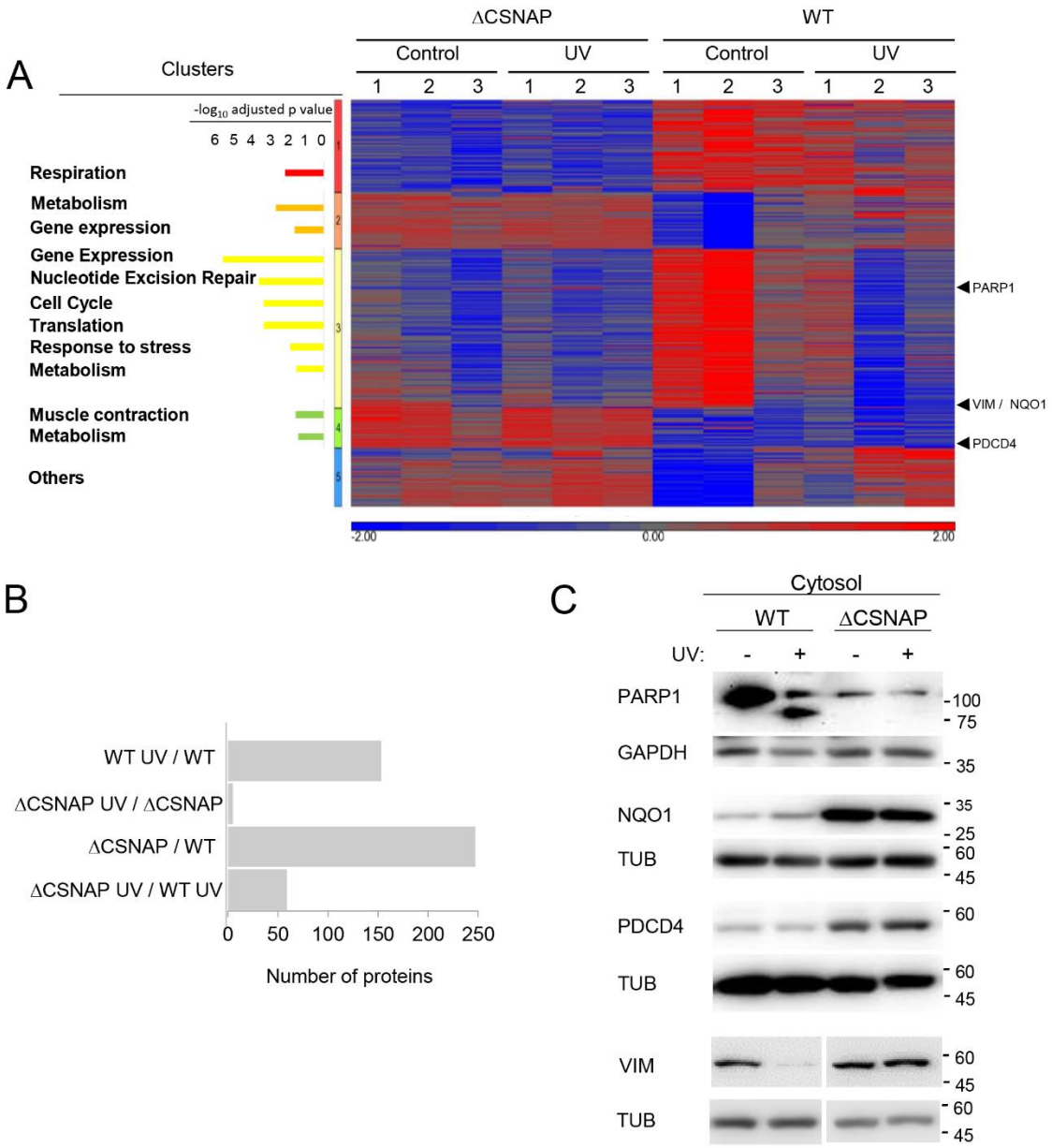

Figure 3. The absence of CSNAP affects proteome remodeling following UV damage.

(A) Proteomes of untreated or UV exposed WT and ΔCSNAP cells four hours post damage were analyzed using label free proteomics approach. Proteomics data of three biological replicates, after logarithmic transformation and flooring, were analyzed by two-way ANOVA using the two factors: strain and UV treatment, as well as their interaction. Proteins with p-value below 0.05 and an absolute fold change above 1.5 were considered as being differentially expressed. Heatmap of differentially expressed proteins grouped to five clusters. Pathway analysis of the clusters indicate up- and downregulation of several cellular functions in ΔCSNAP cells. The bar chart on the left expresses the significance levels of the enrichment analysis of the proteins using the protein coding part of the human genome.

(B) Comparison of the differentially expressed proteins in the proteome in untreated and UV-exposed WT and ΔCSNAP cells. The bar plot shows each of the four pair-wise comparisons, highlighting that in ΔCSNAP cells the DNA damage response is compromised.

(C) Expression levels of four representative proteins: PARP1, NQO1, PDCD4, and vimentin, analyzed by Western blots of WT and ΔCSNAP cell lysates.

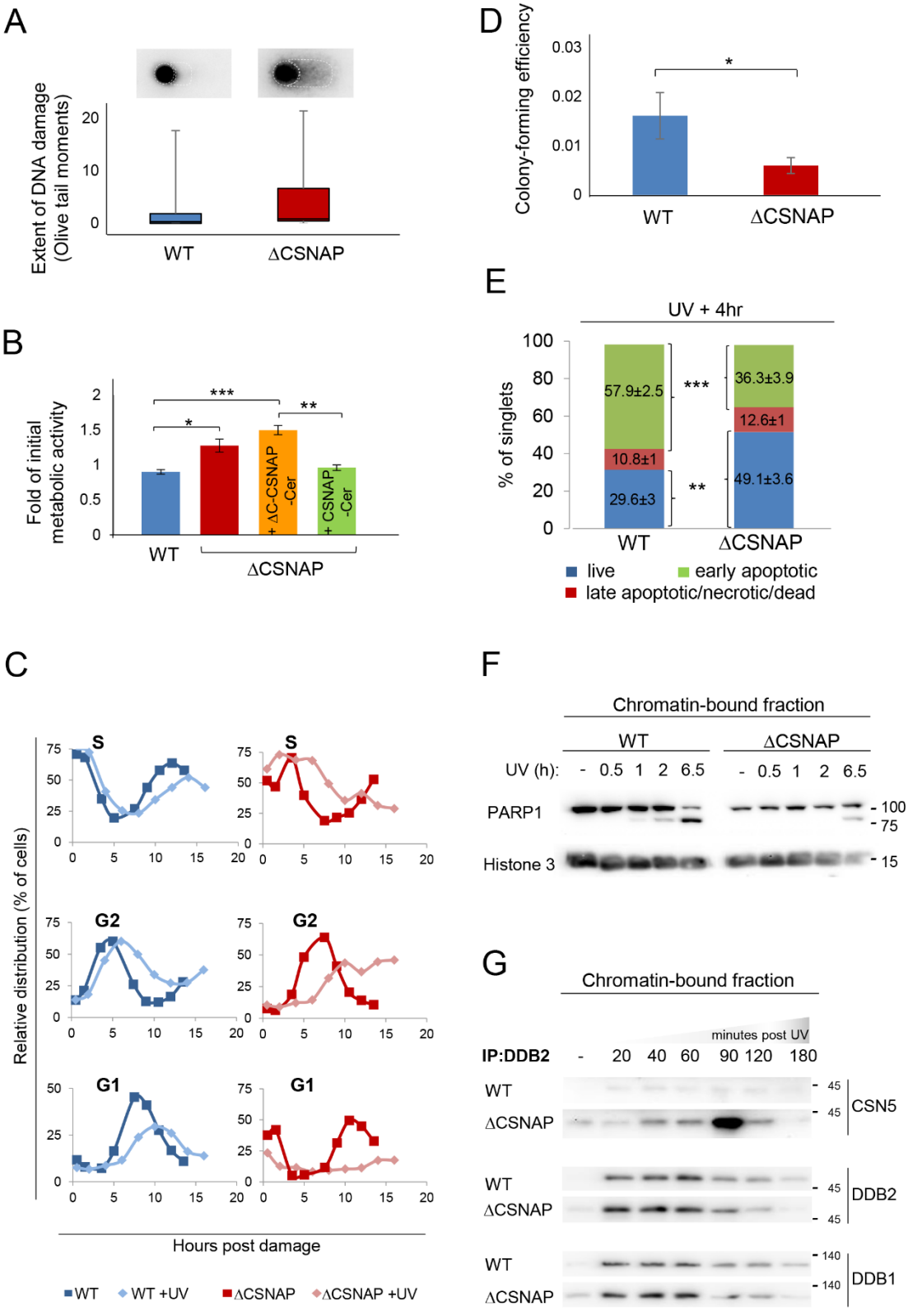

Figure 4. The absence of CSNAP compromises the DNA damage response.

(A) Unlike WT cells, damaged DNA accumulates in ΔCSNAP cells following UV exposure. The genotoxic effect of UV was measured using an alkaline comet assay. DNA damage, expressed as Olive tail moments were calculated and presented as a box-whisker plot. Images above the plot display a representative comet shape for each cell type.

(B) ΔCSNAP cells fail to downregulate their metabolic activity after UV-induced DNA damage. The plot shows metabolic activities of WT and ΔCSNAP cells two hours after exposure to UV irradiation, calculated as a fold of initial activity for each cell line. UV-induced DNA damage caused a significant reduction of metabolic activity in WT cells (blue), while cells deficient in CSNAP (red) failed to down-regulate their metabolic activity to that extent. This UV-response phenotype is rescued by exogenous expression of the full-length CSNAP protein (green), but not when its C-terminal CSN-interaction domain was missing (orange). The graph represents the averages of three independent experiments, with standard errors. Significance was calculated using a 2-way ANOVA test, followed by a Tukey Post-Hoc Test ($p<0.005$). (*$p<0.05$; **$p<0.01$; ***$p<0.005$).

(C) UV-exposed ΔCSNAP cells stay longer in S and G2 phases. Comparison of the relative distribution of cell populations in different phases of the cell cycle, as calculated from flow cytometry histograms of double thymidine-synchronized cells, with or without exposure to UV irradiation. UV-caused DNA damage elongates the S and G2 phases; this effect is significantly more pronounced in cells lacking CSNAP.

(D) Cells lacking CSNAP exhibit a compromised recovery after exposure to high-dose UV. WT and ΔCSNAP cells were exposed to UV irradiation, prior to incubation in culturing conditions for 8 days. Colonies were stained and counted. ΔCSNAP cells exhibit ~2.7-fold less colony-forming potential following UV damage, in comparison to WT cells. The graph represents average results from 7 biological replicates with standard errors. Significance was calculated using a Student's t-test ($p<0.05$).

(E) The early apoptotic response is delayed in ΔCSNAP cells, following UV damage. The bar charts represents the percentage of live, early and late apoptotic cells detected by flow cytometry of 6 independent experiments. A significant difference is seen in the percentage of live and early apoptotic cell populations between WT and ΔCSNAP cells, after exposure to UV (***$p<0.0005$ and **$p<0.001$, respectively).

(F) PARP1 cleavage is delayed in cells lacking CSNAP. Chromatin-bound fractions were monitored by Western blot for caspase-mediated PARP1 cleavage, a marker for commitment to apoptosis.

(G) $CSN^{\Delta CSNAP}$ exhibits increased affinity towards DDB2, in comparison to the CSN complex. WT and ΔCSNAP cells were exposed to UV irradiation, and DDB2 was immunoprecipitated from the chromatin-bound fraction at different time points post-UV damage. Western blot analyses show tighter CSN-CRL binding when CSNAP is absent. Representative blot out of four repeats.

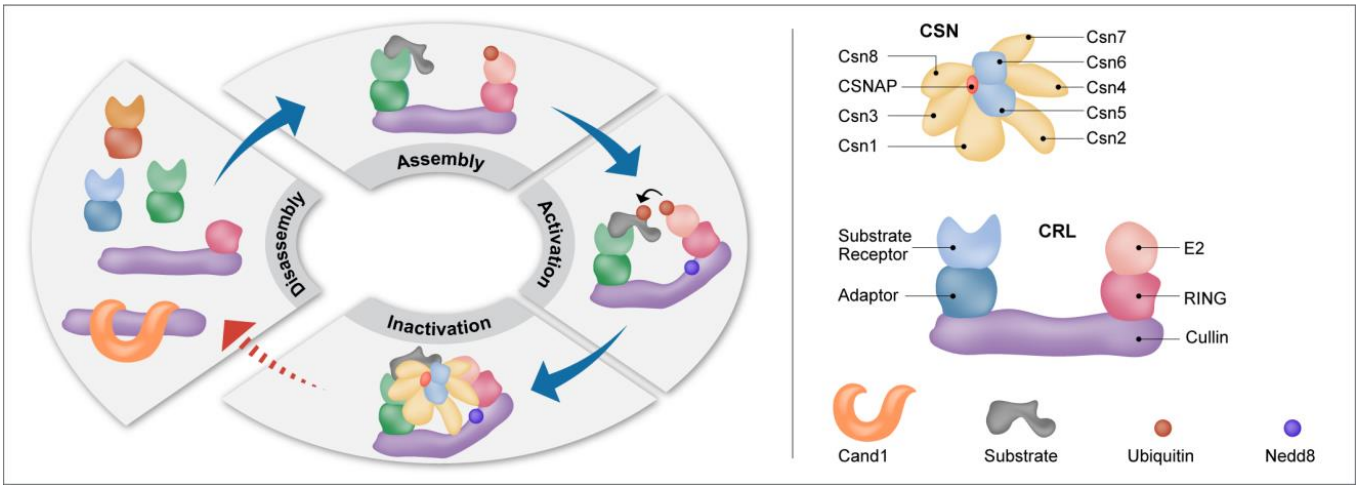

Figure 5. CSNAP influences the strength of the CSN-CRL interaction.
Diagram representing the CRL cycle. CRLs form dynamic complexes with various adaptors and substrate receptors. The conjunction of Nedd8 to a conserved lysine residue in the cullin subunit, induces a conformational change that activates the CRL complex, promoting ubiquitin transfer to the substrate. The CSN complex inactivates CRL assemblies by two independent mechanisms, catalytic and non-catalytic. The first involves catalytic removal of the Nedd8 conjugate, while the second is mediated through physical binding to CRLs, sterically precluding interactions with E2 enzymes and ubiquitination substrates. Subsequently, after CSN dissociation, CRLs can be disassembled and assembled into new configurations, or bind Cand1. This cycle enables CRL adaptation according to cellular need, enabling specific substrates to be ubiquitinated. Our results indicate that CSNAP reduces the affinity of CSN for CRL, thus enabling efficient disassembly and remodeling of CRL complexes. In the absence of CSNAP, the disassembly and assembly steps of the cycle are compromised, as designated by the red dashed lines, affecting the reconfiguration of CRL assemblies, and their ability to respond to cellular stimuli.

Supplemental Information

Supplemental Figures

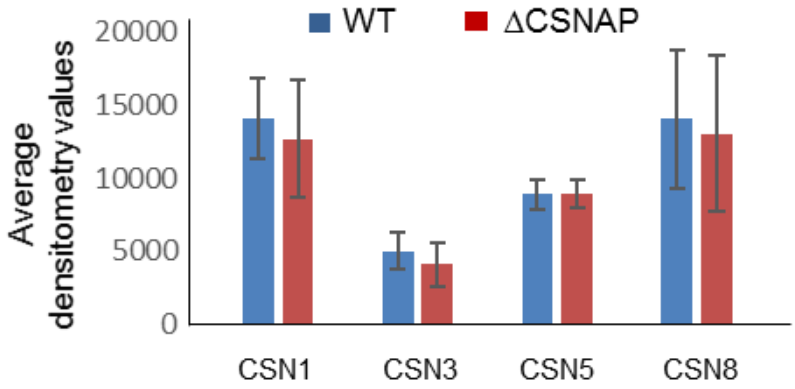

Figure S1. The levels of CSN subunits are comparable in WT and ΔCSNAP cells. Quantification of CSN subunit levels from three independent experiments with standard errors. (see Fig.1D).

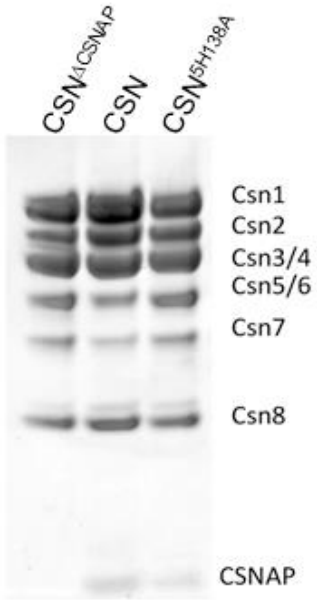

Figure S2. Recombinant CSN complexes. Purified WT and mutant ($CSN5^{H138A}$) CSN complexes expressed with or without CSNAP in insect cells**.**

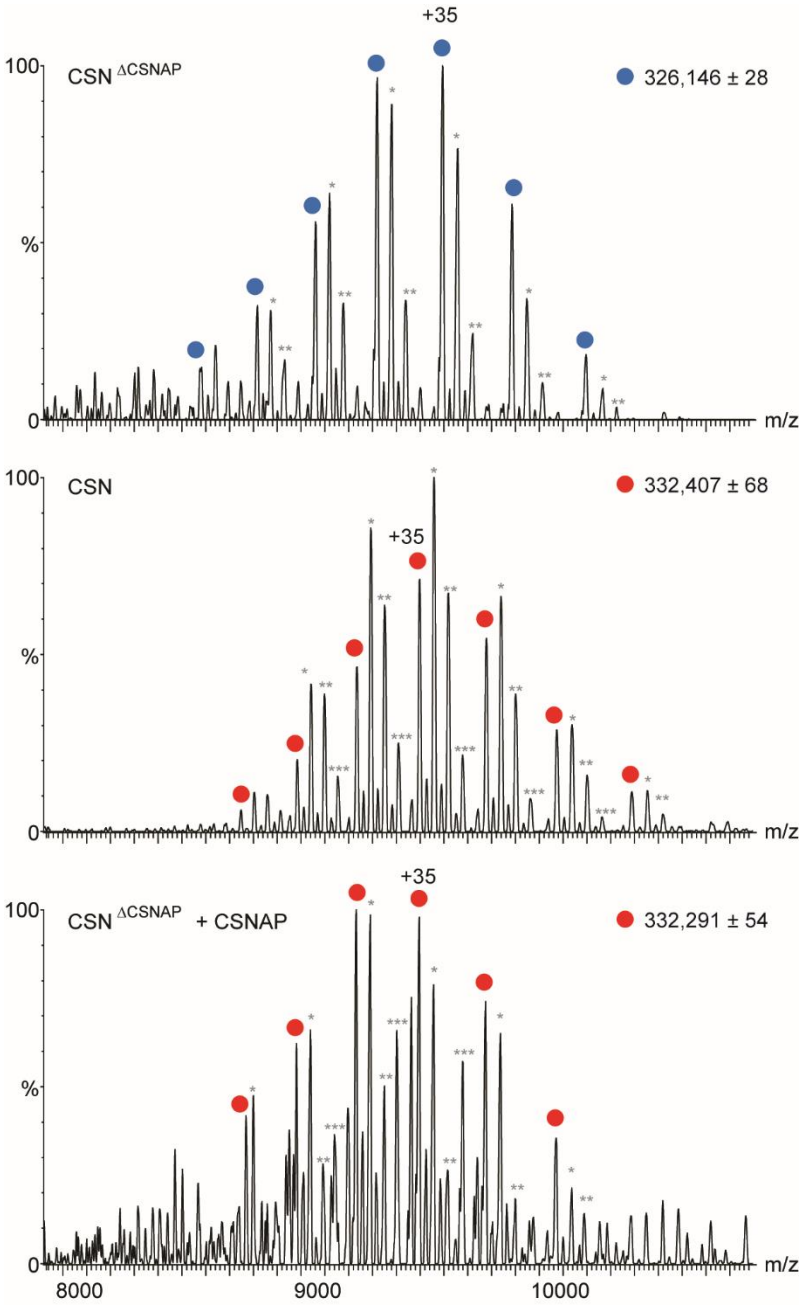

Figure S3. Recombinant CSN and CSN$^{\Delta CSNAP}$ complexes form intact complexes. Native mass spectrometry analysis of recombinant CSN complexes, purified from insect cells. The mass difference between CSN$^{\Delta CSNAP}$ (top panel, blue circles) and CSN (middle panel, red circles) coincides nicely with the mass of CSNAP, indicating that the intact complex contains a single and stoichiometric CSNAP subunit. The bottom panel shows that when the CSN$^{\Delta CSNAP}$ is supplemented with a synthetic CSNAP peptide, it is reconstituted into the intact, CSN complex (red circles). Asterisks indicate populations with purification adducts.

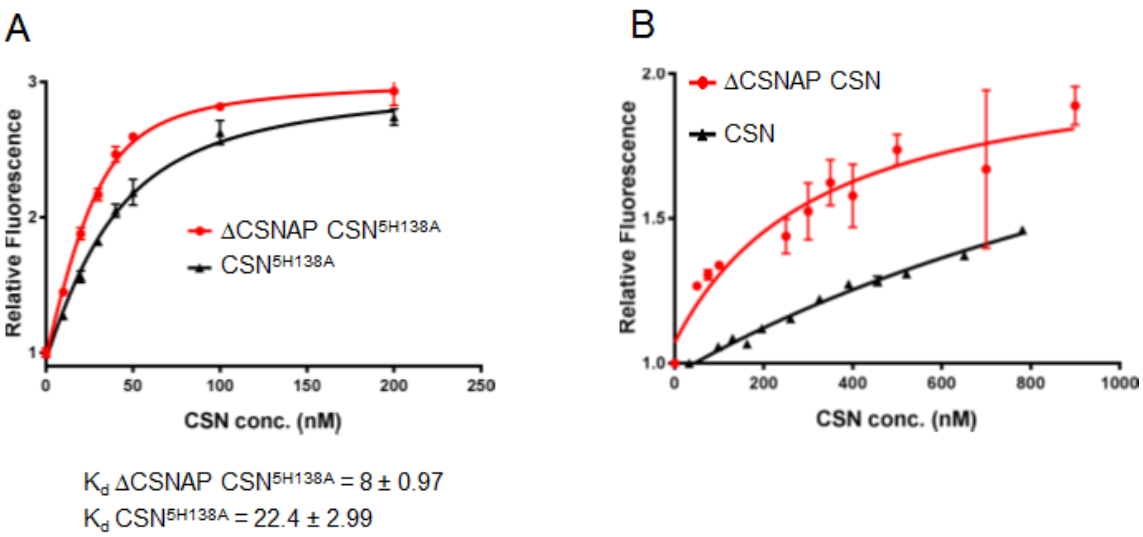

Figure S4. The absence of CSNAP increases the affinity towards Cul1. K_d for CSN and CSN$^{\Delta CSNAP}$ complexes were determined by measuring the change in dansyl fluorescence using the well characterized H138A CSN5 mutation (CSN^{5H138A}) (A), the WT CSN5 subunit (B), and the dansyl-labeled Cul1-N8/Rbx1CSN complexes. All binding measurements were carried out in triplicate and error bars represent standard deviation.

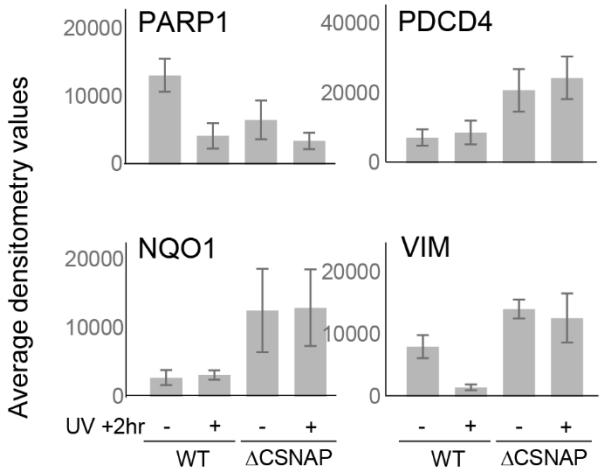

Figure S5. Differences in protein expression levels among WT and ΔCSNAP cells. Densitometry analysis of PARP1, PDCD4, NQO1 and vimentin (shown in Fig.3C). Values are average of three independent experiments; error bars represent standard errors.

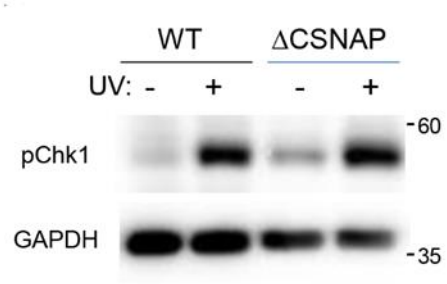

Figure S6. Checkpoint control is unaffected in cells lacking CSNAP. Untreated and UV-exposed WT and ΔCSNAP cells were lysed four hours post-damage, and phosphorylation of Chk1 (Ser345) was compared. In response to UV irradiation, Chk1 is phosphorylated, as expected. Thus, phosphorylation of Chk1 is not affected in cells lacking CSNAP.

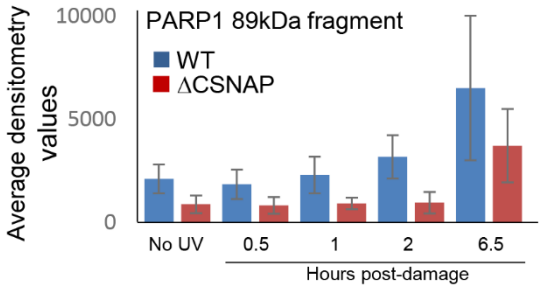

Figure S7. PARP1 cleavage is delayed in ΔCSNAP cells. Densitometry analysis of the full length PARP1 and its 89 kDa cleavage fragment (shown in Fig.4F). Values are average of three independent experiments; error bars represent standard errors.

Table S1.

Proteins significantly enriched in ΔCSNAP cells in comparison to WT cells, yielded by label-free proteomic analysis following immunoprecipitation through CSN3. ($-\log_{10}$ p value>1.3; $\log_2$ fold changes x < -0.58 (blue) and x > 0.58 (red)).

Uniprot accession number	Gene name	$\log_2$ fold change	$-\log_{10}$ pvalue	Uniprot accession number	Gene name	$\log_2$ fold change	$-\log_{10}$ pvalue
Q9BWD1	THIC	1.6956	3.9743	P00338	LDHA	1.8883	1.8427
E9PAV3	NACAM	1.2499	3.8691	P54886	P5CS	1.0391	1.8344
P30101	PDIA3	1.9078	3.7493	Q92598	HS105	1.6920	1.8193
Q12768	STRUM	6.3910	3.7293	P33993	MCM7	0.9122	1.8149
P21333	FLNA	1.8552	3.6539	O15372	EIF3H	0.7536	1.8098
O15371	EIF3D	0.8993	3.1860	P41250	SYG	0.9340	1.8017
P49327	FAS	0.7462	3.1176	P24534	EF1B	1.9708	1.8007
P04075	ALDOA	1.2162	3.1069	Q9H9Z2	LN28A	3.0112	1.7964
Q15370	ELOB	0.8874	3.0951	P62937	PPIA	1.2239	1.7913
Q93034	CUL5	3.5982	3.0728	P06454	PTMA	2.3403	1.7792
Q99873	ANM1	0.8659	3.0266	Q32Q12	Q32Q12	1.2562	1.7755
P06733	ENOA	1.2707	2.9685	Q99714	HCD2	1.3991	1.7581
Q16181	SEPT7	1.7359	2.9223	P0DME0	SETLP	1.6546	1.7529
Q7KZF4	SND1	3.0736	2.8969	Q13283	G3BP1	2.1654	1.7506
P04637	P53	3.4903	2.8196	P14174	MIF	0.7318	1.7368
P62258	1433E	1.8597	2.8097	P55795	HNRH2	1.1718	1.7286
P23588	IF4B	4.8089	2.7430	P22314	UBA1	0.8795	1.7200
I3L398	I3L398	1.9751	2.6830	P11586	C1TC	0.8580	1.7166
Q53GT1	KLH22	2.0972	2.6360	P27797	CALR	1.5285	1.7156
P52907	CAZA1	1.9702	2.6159	Q99832	TCPH	0.7600	1.6966
P07737	PROF1	1.0753	2.5551	Q6P5R6	RL22L	1.7028	1.6745
P22061	PIMT	1.2086	2.5231	P55884	EIF3B	0.7417	1.6742
Q15369	ELOC	0.7892	2.5221	P23528	COF1	1.6341	1.6728
Q05639	EF1A2	1.5172	2.5025	P26641	EF1G	1.5059	1.6689
P61604	CH10	1.2258	2.4741	Q96PM5	ZN363	2.1172	1.6633
Q9Y617	SERC	2.8439	2.4724	P68104	EF1A1	0.7885	1.6427
P31948	STIP1	0.9790	2.4717	Q92466	DDB2	1.6270	1.6270
Q641Q2	FA21A	2.7654	2.4495	Q15181	IPYR	1.1093	1.6133
P15311	EZRI	1.8710	2.3423	P08670	VIME	1.5268	1.6083
P48444	COPD	1.8732	2.3258	P60900	PSA6	0.8485	1.6003
Q8IZP2	ST134	0.9242	2.3218	Q13813	SPTN1	1.2600	1.5924
P61586	RHOA	0.8625	2.3170	Q06830	PRDX1	1.0270	1.5921
B7Z596	B7Z596	4.2825	2.2909	P68032	ACTC	1.4432	1.5658
P63104	1433Z	1.7811	2.2172	P39019	RS19	0.9037	1.5432
Q86VP6	CAND1	1.0216	2.1308	Q9Y3F4	STRAP	0.7431	1.5271
P60891	PRPS1	1.1298	2.0994	P21741	MK	3.5742	1.5117
P14618	KPYM	0.8056	2.0897	P48643	TCPE	0.9243	1.4827
P63208	SKP1	2.1534	2.0827	O43707	ACTN4	2.7602	1.4384
P40926	MDHM	1.5193	2.0800	Q9P2E9	RRBP1	1.1648	1.4319
P08195	4F2	1.2258	2.0463	P11021	GRP78	0.7616	1.4106
P22234	PUR6	1.1621	2.0286	P30041	PRDX6	1.3424	1.4058
Q01518	CAP1	2.2228	2.0160	P53396	ACLY	0.9641	1.4030
Q9Y490	TLN1	0.9604	1.9847	Q9BXJ9	NAA15	0.8394	1.3950
P27348	1433T	1.0527	1.9811	P05455	LA	0.7491	1.3695
A0A087X1X7	A0A087X1X7	1.6393	1.9653	P18085	ARF4	0.8230	1.3638
P50454	SERPH	1.4891	1.9633	P62249	RS16	1.0249	1.3575
Q9Y266	NUDC	1.3480	1.9620	O60841	IF2P	2.4468	1.3552
Q9NWX5	ASB6	2.4333	1.9511	P08708	RS17	0.8600	1.3551
Q96EF6	FBX17	2.6532	1.9471	P29401	TKT	1.5575	1.3528
P00558	PGK1	1.0668	1.9307	P53582	MAP11	-25.0334	2.9375
Q15084	PDIA6	1.5511	1.9017	Q9BX70	BTBD2	-2.4283	2.7711
P55010	IF5	3.3451	1.8958	Q9H0C5	BTBD1	-3.2999	2.6995
P39687	AN32A	0.9212	1.8950	Q8WV16	DCAF4	-0.8846	1.4444
P07195	LDHB	1.4921	1.8915	P35573	GDE	-0.6667	1.4231
Q9H469	FXL15	4.7043	1.8487	Q8WXF1	PSPC1	-0.6875	1.3492
P07355	ANXA2	1.2059	1.8466				

Table S2A.

The table shows the differentially ubiquitinated proteins obtained in at least two out of four experiments, with $\log_2$ fold change (ΔCSNAP / WT) above 1.5 in SILAC proteomic analysis.

Gene Name	Uniprot accession number	Gene Name	Uniprot accession number	Gene Name	Uniprot accession number
OGT	O15294	**RPS3**	P23396	**SLC1A4**	P43007
KIF1A	Q12756	**NBR1**	Q14596	**MAP1B**	P46821
USP9X	Q93008	**HIF1A**	Q16665	**VAMP7**	P51809
TOM1	O60784	**HSD17B12**	Q53GQ0	**SLC12A2**	P55011
RPN1	P04843	**PI4K2A**	Q9BTU6	**YBX1**	P67809
SLC3A2	P08195	**SMAP**	O00193	**SLC7A5**	Q01650
VIM	P08670	**BSG**	P35613	**TRAF2**	Q12933
PARP1	P09874	**SLC19A1**	P41440	**TRAF3**	Q13114
XRCC5	P13010	**SLC6A8**	P48029	**PEG10**	Q86TG7
RBMX	P38159	**ACLY**	P53396	**APH1B**	Q8WW43
PEX19	P40855	**SLC16A1**	P53985	**EPS15L1**	Q9UBC2
NEDD4	P46934	**RAD23A**	P54727	**VTI1B**	Q9UEU0
UBE2N	P61088	**RAD23B**	P61956	**SSR3**	Q9UNL2
RAB1A	P62820	**YWHAZ**	P63104	**ATXN10**	Q9UBB4
VAMP2	Q15836	**MSMO1**	Q15800	**HIST1H1E**	P10412
PPP2CA	P62714	**CCDC50**	Q8IVM0	**HIST1H1C**	P16403
ZMYM3	Q14202	**ARL8A**	Q96BM9	**ARL8B**	Q9NVJ2
PCM1	Q14202	**ITCH**	Q96J02	**UBXN7**	O94888
STX12	Q15154	**FANCI**	Q9NVI1	**FADS2**	O95864
ANKRD13A	Q8IZ07	**NSFL1C**	Q9UNZ2	**PCNA**	P12004
PDCD6IP	Q8WUM4	**ERH**	P84090	**BCAP31**	P51572
SERINC1	Q9NRX5	**SLC1A5**	Q15758	**RPS27A**	P62979
CEP131	Q9UPN4	**SMIM14**	Q96QK8	**WLS**	Q5T9L3
EPN1	Q9Y6I3	**MAGED1**	Q9Y5V3	**MIB1**	Q86YT6
STAM2	O75886	**SCAMP1**	O15126	**SLC29A1**	Q99808
ATP1A1	P05023	**CALM3**	P0DP25		
ITGB1	P05556	**HSPA8**	P11142		

Table S2B.

The table shows the differentially ubiquitinated proteins obtained in at least two out of four experiments, with $\log_2$ fold change (ΔCSNAP / WT) below 0.67 in SILAC proteomic analysis

Gene Name	Uniprot accession number	Gene Name	Uniprot accession number	Gene Name	Uniprot accession number
TYMS	P04818	**HDAC1**	Q13547	**GINS1**	Q14691
MCM4	P33991	**NCOA4**	Q13772	**ARMC6**	Q6NXE6
SHMT1	P34896	**PCBP2**	Q15366	**C15orf39**	Q6ZRI6
ITM2B	Q9Y287	**RBBP7**	Q16576	**TMEM57**	Q8N5G2
RGPD3	P49792	**TTI2**	Q6NXR4	**PDCD7**	Q8N8D1
ORC5	O43913	**VWA1**	Q6PCB0	**SPG11**	Q96JI7
TPT1	P13693	**NOP9**	Q86U38	**TRIM47**	Q96LD4
RCC1	A6NED2	**DNAAF5**	Q86Y56	**PHB2**	Q99623
NSG1	P42857	**SCAF11**	Q99590	**BCL2L12**	Q9HB09
IREB2	P48200	**DUSP9**	Q99956	**ITM2C**	Q9NQX7
MYL6	P60660	**ANP32E**	Q9BTT0	**AAAS**	Q9NRG9
ZBTB33	Q86T24	**RNPEP**	Q9H4A4	**RNF216**	Q9NWF9
AEN	Q8WTP8	**ZNF281**	Q9Y2X9	**SMPD4**	Q9NXE4
GCN1L1	Q92616	**MTCH2**	Q9Y6C9	**DPP7**	Q9UHL4
SEC11C	Q9BY50	**PRMT5**	O14744	**CDC23**	Q9UJX2
ALG13	Q9NP73	**CCNB2**	O95067	**RUVBL1**	Q9Y265
KDM5B	Q9UGL1	**NDUFB10**	O96000	**TMX2**	Q9Y320
TELO2	Q6NXR4	**ENO1**	P06733	**HMGCR**	P04035
NBPF19	A0A087WUL8	**HSP90AB1**	P08238	**PSMA4**	P25789
PHGDH	O43175	**CDK4**	P11802	**PSMC2**	P35998
PSMD3	O43242	**ATP2A2**	P16615	**RPS19**	P39019
EEF1G	P26641	**POLR2C**	P19387	**AP3M2**	Q9Y2T2
RPL3	P18077	**POLR2A**	P24928	**SPG20**	Q8N0X7
RPL28	P46779	**PSMB6**	P28072	**FANCI**	Q9NVI1
FNTB	P49356	**QARS**	P47897	**ARIH1**	Q9Y4X5
NDUFA8	P51970	**CORO7**	P57737	**DDX39A**	O00148
HNRNPM	P52272	**AP3S2**	P59780	**GNAS**	P63092
THOP1	P52888	**DAD1**	P61803	**TBCD**	Q9BTW9
CAPZA1	P52907	**RPL23**	P62829	**OTUD5**	Q96G74
RABGGTB	P53611	**EIF5A**	P63241	**MAGOH**	P61326
SUMO2	P61956	**NUP160**	Q12769	**NCAPD2**	Q15021
RPS11	P62280	**ILF2**	Q12905	**HSPH1**	Q92598
SEC11A	P67812	**EIF4A2**	P60842	**MSTO1**	Q9BUK6

Gene Name	Uniprot accession number	Gene Name	Uniprot accession number
ITM2A	O43736	**PSMB2**	P49721
DHFR	P00374	**ATP1B3**	P54709
LDHB	P07195	**PMPCA**	Q10713
GLUL	P15104	**HAX1**	O00165
RPS2	P15880	**DEGS1**	O15121
UQCRC2	P22695	**RNASEH2A**	O75792
RPL10	P27635	**RPL13A**	P40429
CAD	P27708	**RPS10**	P46783
PSMB4	P28070	**PLA2G16**	P53816
POLD1	P28340	**RPS20**	P60866
PPP1CC	P36873	**TRIM28**	Q13263
EIF2S3	P41091	**CNOT11**	Q9UKZ1
RPS27	P42677	**PSMD14**	O00487
TSC2	P49815	**PFAS**	O15067
USP14	P54578	**GAPDH**	P04406
ATP6V0D1	P61421	**HSPB1**	P04792
RPS23	P62266	**PKM**	P14618
RPL11	P62913	**RPS3**	P23396
GNB2L1	P63244	**MCM7**	P33993
POU5F1	Q01860	**CCT3**	P49368
GTF2H3	Q13889	**EIF3E**	P60228
PMF1	Q6P1K2	**EIF4A1**	P60842
WDR74	Q6RFH5	**EEF1A1**	P68104
CCAR2	Q8N163	**PRKDC**	P78527
SARAF	Q96BY9	**EIF3I**	Q13347
VPS25	Q9BRG1	**NONO**	Q15233
ITPA	Q9BY32		
WDR33	Q9C0J8		
UTP6	Q9NYH9		
DTL	Q9NZJ0		
HDAC9	Q9UKV0		
C14orf166	Q9Y224		
LDHA	P00338		

Table S3. Known CRL substrates identified in SILAC-based ubiquitination analysis of WT and ΔCSNAP cells. Based on references (1)(Emanuele et al., 2011), (2)[21], (3)[22], and (4)[23].

Differentially ubiquitinylated CRL substrates in WT and ΔCSNAP cells			References	GO Annotation / Pathway (Biological process / Molecular Function*)		CRL substrate
ΔCSNAP / WT down-regulated	TYMS		1	DNA biosynthetic process	GO:0071897	
	MCM4		1	DNA replication	GO:0006260	
	IREB2		1	Metabolic process	GO:0008152	
	KDM5B		1	Histone H3-K4 demethylation	GO:0034720	
	PHGDH		1	Electron transport chain	GO:0022900	
	PSMD3		1	Ubiquitin-dependent protein catabolic process	GO:0006511	
	RPL3		1,2	Translation	GO:0006412	CRL1
	HNRNPM		1	mRNA splicing, via spliceosome	GO:0000398	
	ENO1		1	Negative regulation of cell growth	GO:0030308	
	POLR2C		1	Dual incision in TC-NER	R-HSA-6782135	
	POLR2A		1	Dual incision in TC-NER	R-HSA-6782135	
	RNF216		1	Apoptotic process	GO:0006915	
	PSMA4		1	Proteasome	hsa03050+5685	
	PSMC2		1	Proteasome	hsa03050+5701	
	ARIH1		1	Protein polyubiquitination	GO:0000209	
	OTUD5		1	Protein deubiquitination	GO:0016579	
	LDHB		1	Oxidation-reduction process	GO:0055114	
	GLUL		1	Cell proliferation	GO:0008283	
	UQCRC2		1	Aerobic respiration	GO:0009060	
	PPP1CC		1	Cell division	GO:0051301	
	DTL		1,2,4	Cellular response to DNA damage stimulus	GO:0006974	CRL1, CRL2/CRL4
	PSMB2		1	Proteasome	hsa03050+5690	CRL1
	TRIM28		1	DNA repair	GO:0006281	
	PFAS		1	Metabolic pathways	hsa01100+5198	
	GAPDH		1	Metabolic pathways	hsa01100+2597	
	RPS3		1	Apoptotic process	GO:0006915	
	MCM7		1,4	Cell proliferation	GO:0008283	CRL4,CRL2
	PRKDC		1	Cell proliferation	GO:0008283	
	EIF3I		1	Translational initiation	GO:0006413	
	NONO		1,2	DNA repair	GO:0006281	CRL1
	CDC23		1	Cell division	GO:0051301	CRL3
	TPT1		2	Cell differentiation	GO:0030154	CRL1
	EEF1G		2	Eukaryotic Translation Elongation	R-HSA-156842	CRL1
	CDK4		2	Cell division	GO:0051301	CRL1
	QARS		2	Metabolic pathways	hsa01100+5859	CRL1

Differentially ubiquitinylated CRL substrates in WT and ΔCSNAP cells		References	GO Annotation / Pathway (Biological process / Molecular Function*)		CRL substrate
ΔCSNAP / WT down-regulated	ITM2C	4	Positive regulation of extrinsic apoptotic signaling pathway	GO:2001238	CRL2
	SMPD4	4	Metabolic pathways	hsa01100+55627	CRL2
	GNB2L1	3,4	Apoptotic process Cell cycle	GO:0006915 GO:0007049	CRL1, CRL2/CRL4
	HSP90AB1	1	Negative regulation of proteasomal ubiquitin-dependent protein catabolic process	GO:0032435	
	RPL13A	1	Translation	GO:0006412	
	NCAPD2	4	Cell division	GO:0051301	CRL2
	AAAS	4	Nucleocytoplasmic transport	GO:0006913	CRL4
	GNAS	4			CRL4
	DPP7	2	Proteolysis	GO:0006508	CRL1
	RPS2	2	Translation	GO:0006412	CRL1, CRL4
	HAX1	2	Regulation of apoptotic process	GO:0042981	CRL1
	RBBP7	4	Cell proliferation	GO:0008283	CRL2/CRL4
	CORO7	4	Protein transport	GO:0015031	CRL2/CRL4
	ARMC6	4			CRL2
	PHB2	4	Positive regulation of cell cycle G1/S phase transition	GO:1902808	CRL2

*GO Annotation Molecular Function

Differentially ubiquitinylated CRL substrates in WT and ΔCSNAP cells		References	GO Annotation / Pathway (Biological process)		CRL substrate
ΔCSNAP / WT up-regulated	PEX19	1	Peroxisome	hsa04146+5824	
	PPP2CA	1	Apoptotic process	GO:0006915	
	EPN1	1	Endocytosis	hsa04144+29924	
	RPS3	1	Apoptotic process Cell division DNA repair	GO:0006915 GO:0051301 GO:0006281	
	HIF1A	1,3	Neddylation	R-HSA-8951664	CRL1
	PI4K2A	1	Metabolic pathways	hsa01100+55361	
	RAD23B	1	Nucleotide-excision repair	GO:0006289	
	HSPA8	1	Regulation of cell cycle	GO:0051726	
	YBX1	1	Positive regulation of cell division	GO:0051781	
	HIST1H1C	1			
	UBXN7	1	Neddylation	R-HSA-8951664	
	BCAP31	1	Apoptotic cleavage of cellular proteins	R-HSA-111465	
	MIB1	1	Protein ubiquitination	GO:0016567	
	RPN1	2	Metabolic pathways	hsa01100+6184	CRL1
	UBE2N	4	Positive regulation of DNA repair	GO:0045739	CRL2/CRL4
	MAGED1	3	Regulation of apoptotic process	GO:0042981	CRL1
	RAD23A	1	Nucleotide-excision repair	GO:0006289	
	CALM3	2			CRL1
	SLC6A8	4	Transport	GO:0006810	CRL4

Table S4.

Differentially ubiquitinated proteins linked to cell cycle that were identified by SILAC-based analysis of WT and ΔCSNAP cells. Known CRL substrates are indicated based on the following references (1)(Emanuele et al., 2011), (2)[21], (3)[22], and (4)[23].

	Uniprot accession number	Gene name	CRL substrate	Reference
ΔCSNAP / WT down-regulated	Q14691	GINS1		
	P33993	MCM7	CRL4, CRL2	2,4
	O00487	PSMD14		
	Q13547	HDAC1		
	Q9NRG9	AAAS	CRL4	4
	P04818	TYMS		
	Q6P1K2	PMF1		
	Q12769	NUP160		
	P00374	DHFR		
	P28072	PSMB6		
	O43913	ORC5		
	P36873	PPP1CC		
	O95067	CCNB2		
	P28070	PSMB4		
	P25789	PSMA4		
	Q9UJX2	CDC23	CRL3	2
	P42677	RPS27		
	P49721	PSMB2	CRL1	1
	P11802	CDK4	CRL1	1
	P28340	POLD1		
	P35998	PSMC2		
	O43242	PSMD3		
	P33991	MCM4		
	Q15021	NCAPD2	CRL2	4
	P08238	HSP90AB1		
	Q9Y265	RUVBL1		
	Q16576	RBBP7	CRL2/CRL4	4
ΔCSNAP / WT up-regulated	P62714	PPP2CA		
	P62820	RAB1A		
	Q15154	PCM1		
	P12004	PCNA		
	Q9UPN4	CEP131		
	P61088	UBE2N	CRL2/CRL4	4
	P62979	RPS27A		
	P63104	YWHAZ		

Table S5.

Pathway analysis using Reactome 2016 of differentially ubiquitinylated proteins. Tables A and B display proteins exhibiting a ΔCSNAP/WT fold change bigger than 1.5 (A) or smaller then 0.66 (B).

The tables are provided as separate excel files.

Table S6A.

Proteins that were significantly differentially expressed between ΔCSNAP and WT cells, as demonstrated by total proteome label-free proteomic analysis. ($-\log_{10}$ p value>1.3; $\log_2$ fold changes x < -0.585 (blue) and x > 0.585 (red)).

Uniprot Accession number	Uniprot Gene Name	-log10 p value	log2 ΔCSNAP/WT ratio	Uniprot Accession number	Uniprot Gene Name	-log10 p value	log2 ΔCSNAP/WT ratio
P00966	ASS1	1.308	4.719	Q5UIP0	RIF1	1.716	1.132
Q14534	SQLE	1.974	4.716	P50454	SERPINH1	1.651	1.130
Q96P11	NSUN5	1.480	4.530	P17612	PRKACA	1.829	1.125
Q15274	QPRT	1.504	3.544	K7ERP4	GPX4	1.752	1.111
Q04760	GLO1	1.358	2.472	P55081	MFAP1	1.303	1.095
P04818	TYMS	1.461	2.319	E7EX44	CALD1	1.371	1.068
Q9Y3D6	FIS1	1.556	2.288	Q96DG6	CMBL	1.385	1.062
O00743	PPP6C	1.346	2.196	O95864	FADS2	1.346	1.058
P49755	TMED10	1.485	1.918	P19525	EIF2AK2	1.467	1.046
Q8WVY7	UBLCP1	1.464	1.894	Q709C8	VPS13C	1.474	1.042
P08670	VIM	3.110	1.865	Q6P3X3	TTC27	1.707	1.014
Q9Y2L1	DIS3	1.511	1.859	O95881	TXNDC12	2.422	1.008
Q9NRN7	AASDHPPT	1.538	1.776	P15311	EZR	2.014	1.008
A0A087X1N8	SERPINB6	1.906	1.771	Q9BPU6	DPYSL5	2.256	1.001
Q9Y6C9	MTCH2	1.394	1.758	Q14914	PTGR1	1.649	0.993
O00625	PIR	1.841	1.758	H0Y8C2	RPL22L1	1.615	0.982
Q9UBT2	UBA2	1.439	1.747	Q10713	PMPCA	1.568	0.940
Q9NR31	SAR1A	1.627	1.737	O60869	EDF1	1.598	0.930
O43347	MSI1	1.494	1.661	P22626	HNRNPA2B1	1.369	0.902
Q9H6F5	CCDC86	1.529	1.633	P48163	ME1	1.630	0.894
P15559	NQO1	3.630	1.573	P55010	EIF5	1.371	0.875
P23258	TUBG1	1.770	1.547	P62906	RPL10A	1.301	0.845
Q16763	UBE2S	1.332	1.487	Q7Z3B4	NUP54	1.496	0.834
O94760	DDAH1	2.471	1.459	P61163	ACTR1A	2.081	0.796
Q15293	RCN1	5.125	1.447	Q07065	CKAP4	1.337	0.789
Q3ZCW2	LGALSL	1.864	1.444	Q96F86	EDC3	1.600	0.789
P49137	MAPKAPK2	1.990	1.443	P19367	HK1	1.646	0.786
ALBU_BOVIN		1.786	1.418	P08133	ANXA6	2.197	0.766
A0A0B4J2G4	LRRC41	2.473	1.418	Q5JWF2	GNAS	2.124	0.722
P60903	S100A10	1.725	1.380	Q9Y6B6	SAR1B	1.570	0.708
P14174	MIF	1.406	1.378	P54578	USP14	1.639	0.705
P21291	CSRP1	2.877	1.378	P78318	IGBP1	1.313	0.694
P62995	TRA2B	1.516	1.354	Q99459	CDC5L	1.619	0.674
O15144	ARPC2	1.318	1.344	Q9P0L0	VAPA	2.340	0.672
Q15067	ACOX1	1.344	1.331	Q9NPJ3	ACOT13	1.995	0.632
P09429	HMGB1	1.934	1.292	Q9H8S9	MOB1A	1.530	0.610
P48735	IDH2	2.091	1.284	Q13501	SQSTM1	1.776	0.600
P62805	HIST1H4A	1.653	1.250	Q13347	EIF3I	2.137	0.596
P53004	BLVRA	1.869	1.249	P62714	PPP2CB	1.311	-0.598
O75506	HSBP1	1.935	1.243	Q96HS1	PGAM5	1.629	-0.602
O60282	KIF5C	2.815	1.219	P04350	TUBB4A	1.483	-0.620
P54687	BCAT1	1.483	1.217	P30566	ADSL	1.513	-0.628
Q13509	TUBB3	2.074	1.211	Q7Z6Z7	HUWE1	1.631	-0.631
G5E9W8	GYG1	1.865	1.193	Q14444	CAPRIN1	1.624	-0.639
O95782	AP2A1	2.124	1.188	Q9H583	HEATR1	2.621	-0.659
P30043	BLVRB	1.739	1.177	Q04917	YWHAH	1.386	-0.665
P62314	SNRPD1	1.304	1.162	Q9H2W6	MRPL46	3.001	-0.666
Q96AC1	FERMT2	1.324	1.147	Q9BZF1	OSBPL8	1.940	-0.676
Q96QD8	SLC38A2	1.675	1.140	P09382	LGALS1	1.805	-0.685
P60981	DSTN	1.484	1.139	P38606	ATP6V1A	2.258	-0.691

Uniprot Accession number	Uniprot Gene Name	-log10 p value	log2 ΔCSNAP/WT ratio	Uniprot Accession number	Uniprot Gene Name	-log10 p value	log2 ΔCSNAP/WT ratio
P00374	DHFR	1.716	-0.694	Q02818	NUCB1	1.597	-0.879
Q9H0B6	KLC2	1.455	-0.694	P31930	UQCRC1	2.571	-0.882
P35610	SOAT1	1.348	-0.704	P82673	MRPS35	1.372	-0.892
Q5JY65	CRNKL1	1.398	-0.716	Q9BT78	COPS4	2.097	-0.894
O00231	PSMD11	1.776	-0.718	Q15120	PDK3	1.592	-0.895
Q9H3P7	ACBD3	2.432	-0.727	Q8NCF5	NFATC2IP	1.423	-0.896
O95453	PARN	1.388	-0.730	P12268	IMPDH2	2.223	-0.897
Q9NVP1	DDX18	1.783	-0.731	O60287	URB1	1.860	-0.897
Q9Y6V7	DDX49	1.376	-0.732	Q99504	EYA3	1.539	-0.898
Q99956	DUSP9	1.721	-0.734	Q16851	UGP2	1.694	-0.899
Q13011	ECH1	1.680	-0.736	P52788	SMS	1.607	-0.907
P16278	GLB1	1.323	-0.737	P42704	LRPPRC	1.603	-0.908
Q8N8S7	ENAH	1.443	-0.740	P62829	RPL23	1.768	-0.909
P36543	ATP6V1E1	1.956	-0.747	Q9BYG3	NIFK	2.427	-0.909
P49916	LIG3	1.772	-0.761	Q9NW13	RBM28	1.612	-0.911
Q9Y333	LSM2	2.758	-0.765	Q15126	PMVK	1.823	-0.914
Q9GZP4	PITHD1	1.437	-0.766	Q6P161	MRPL54	1.666	-0.918
P07954	FH	1.505	-0.767	P51858	HDGF	1.756	-0.921
Q9BU76	MMTAG2	2.232	-0.770	P23193	TCEA1	1.346	-0.930
P50453	SERPINB9	1.565	-0.773	Q92793	CREBBP	2.281	-0.943
P07900	HSP90AA1	1.552	-0.775	Q9NZB2	FAM120A	1.775	-0.944
Q5HYB6	DKFZp686J1372	1.697	-0.778	Q7Z6E9	RBBP6	1.920	-0.954
Q08211	DHX9	1.373	-0.779	Q9UMX0	UBQLN1	1.792	-0.954
Q9UMX1	SUFU	1.431	-0.780	O95376	ARIH2	1.420	-0.960
Q12802	AKAP13	1.637	-0.788	Q9UH62	ARMCX3	1.340	-0.960
Q5T8P6	RBM26	1.503	-0.797	Q9Y2R4	DDX52	1.441	-0.967
E7EWR4	CSTF2	1.893	-0.800	P49792	RANBP2	1.537	-0.982
Q5JPH6	EARS2	1.587	-0.804	Q6IN85	SMEK1	1.933	-0.985
Q99543	DNAJC2	1.337	-0.807	Q9Y2Q5	LAMTOR2	1.644	-0.994
Q9Y520	PRRC2C	1.789	-0.808	Q9H2M9	RAB3GAP2	1.362	-0.999
Q8NB90	SPATA5	1.997	-0.810	Q9H501	ESF1	2.352	-0.999
Q9NTJ3	SMC4	1.496	-0.810	Q15291	RBBP5	2.213	-1.002
P20248	CCNA2	2.463	-0.811	Q9NY93	DDX56	2.184	-1.007
Q9BTC0	DIDO1	2.293	-0.812	Q7Z5L9	IRF2BP2	1.568	-1.009
Q8WXI9	GATAD2B	1.660	-0.818	Q9NV56	MRGBP	1.530	-1.015
Q9H2G2	SLK	1.797	-0.820	P09874	PARP1	1.879	-1.018
P49189	ALDH9A1	1.581	-0.828	Q16795	NDUFA9	1.953	-1.029
Q9BXP5	SRRT	2.020	-0.829	Q9Y5J1	UTP18	1.550	-1.030
P28331	NDUFS1	1.557	-0.829	P06280	GLA	1.460	-1.054
P17096	HMGA1	1.472	-0.834	Q6IQ49	SDE2	1.840	-1.060
Q9BTA9	WAC	2.073	-0.848	Q09666	AHNAK	1.491	-1.062
Q96CN7	ISOC1	1.630	-0.849	Q96A65	EXOC4	2.019	-1.064
Q86YP4	GATAD2A	1.839	-0.852	O75153	CLUH	1.392	-1.065
Q01860	POU5F1	4.006	-0.858	Q7Z5K2	WAPAL	1.837	-1.076
P26640	VARS	1.494	-0.864	Q9BTX1	NDC1	1.778	-1.080
O14976	GAK	1.336	-0.866	P07814	EPRS	2.033	-1.095
O15381	NVL	1.317	-0.868	Q7Z3K3	POGZ	2.027	-1.101
Q969E8	TSR2	2.851	-0.874	Q9UQR0	SCML2	3.016	-1.101
P33981	TTK	2.553	-0.875	Q9BTT6	LRRC1	2.296	-1.107
P40818	USP8	1.625	-0.877	Q13492	PICALM	1.564	-1.128

Uniprot Accession number	Uniprot Gene Name	-log10 p value	log2 ΔCSNAP/WT ratio
Q5VT52	RPRD2	3.231	-1.130
Q86UK7	ZNF598	1.917	-1.136
P07858	CTSB	1.608	-1.159
Q5HYI8	RABL3	1.994	-1.168
Q15637	SF1	1.720	-1.187
Q15054	POLD3	1.573	-1.218
O95155	UBE4B	1.776	-1.218
P63173	RPL38	1.780	-1.218
P22059	OSBP	2.834	-1.226
Q7Z417	NUFIP2	1.882	-1.233
Q86U38	NOP9	1.398	-1.248
Q5JRA6	MIA3	2.755	-1.248
Q9Y624	F11R	4.020	-1.257
Q96KB5	PBK	3.738	-1.272
O75694	NUP155	1.947	-1.278
Q6PJG6	BRAT1	1.597	-1.283
P54725	RAD23A	1.758	-1.286
Q9NXV6	CDKN2AIP	1.487	-1.291
O75821	EIF3G	1.435	-1.292
Q7Z4Q2	HEATR3	1.316	-1.317
Q96G46	DUS3L	1.416	-1.330
P53634	CTSC	1.795	-1.331
P20020	ATP2B1	1.717	-1.332
Q14146	URB2	1.666	-1.343
Q9BXR0	QTRT1	2.378	-1.432
Q92733	PRCC	2.655	-1.444
Q9H1E3	NUCKS1	2.140	-1.446
P10606	COX5B	3.153	-1.464
Q9NY61	AATF	2.017	-1.578
Q96BW9	TAMM41	1.734	-1.590
Q9NSE4	IARS2	2.714	-1.657
O60504	SORBS3	1.353	-1.699
Q9Y232	CDYL	2.025	-1.712
Q69YH5	CDCA2	2.432	-1.769
Q8IWV8	UBR2	1.366	-1.771
P46100	ATRX	2.227	-1.804
P14927	UQCRB	1.335	-1.880
Q8WUA4	GTF3C2	2.016	-1.880
Q9ULZ3	PYCARD	2.171	-1.978
Q9Y3Z3	SAMHD1	3.794	-2.100
P04083	ANXA1	4.723	-2.331
Q12962	TAF10	1.821	-2.865
O94788	ALDH1A2	4.853	-3.367
Q8WVV4	POF1B	4.639	-3.509
P31271	HOXA13	1.535	-4.089
A6NDU8	C5orf51	1.465	-5.403
Q9BXV9	C14orf142	2.365	-6.103

Table S6B.

Proteins that were significantly differentially expressed between ΔCSNAP and WT cells following UV exposure, as demonstrated by total proteome label-free proteomic analysis. ($-\log_{10}$ p value>1.3; $\log_2$ fold changes x < -0.585 (blue) and x > 0.585 (red)).

Accession	Uniprot Gene Name	-log10 p value	log2 ΔCSNAP/WT ratio	Accession	Uniprot Gene Name	-log10 p value	log2 ΔCSNAP/WT ratio
P05783	KRT18	1.777	6.184	Q01860	POU5F1	2.912	-0.587
Q53EL6	PDCD4	1.603	4.381	O14965	AURKA	1.404	-0.588
P15559	NQO1	4.886	2.360	Q9BTC0	DIDO1	1.815	-0.653
ALBU_BOVIN		2.592	2.023	P50453	SERPINB9	1.394	-0.700
E7EX44	CALD1	2.552	1.883	Q9H6S0	YTHDC2	1.363	-0.747
P05787	KRT8	2.182	1.843	Q16795	NDUFA9	1.378	-0.758
P16455	MGMT	1.895	1.721	O95453	PARN	1.495	-0.777
P48735	IDH2	2.704	1.657	P10606	COX5B	1.706	-0.798
P08670	VIM	2.739	1.624	P20248	CCNA2	2.485	-0.818
A0A0B4J2G4	LRRC41	2.818	1.623	O95302	FKBP9	1.377	-0.836
Q15293	RCN1	4.872	1.338	Q92733	PRCC	1.491	-0.844
O94760	DDAH1	2.253	1.332	Q9BU76	MMTAG2	2.562	-0.883
P48163	ME1	2.419	1.289	P40818	USP8	1.641	-0.885
Q14914	PTGR1	1.900	1.127	Q86WA8	LONP2	2.167	-0.903
P18206	VCL	1.578	1.056	Q9Y624	F11R	3.059	-0.904
Q96QD8	SLC38A2	1.518	1.046	Q96KB5	PBK	2.915	-0.952
P04899	GNAI2	2.320	0.965	Q9ULT8	HECTD1	1.707	-0.975
P50454	SERPINH1	1.343	0.947	P47712	PLA2G4A	1.704	-1.002
O60282	KIF5C	2.190	0.947	Q69YH5	CDCA2	1.360	-1.046
H0Y8C2	RPL22L1	1.364	0.851	Q9NSE4	IARS2	1.752	-1.090
P15311	EZR	1.579	0.811	Q5T4S7	UBR4	2.242	-1.129
P19367	HK1	1.593	0.764	Q9BW92	TARS2	1.546	-1.156
P45973	CBX5	2.359	0.741	P20020	ATP2B1	2.172	-1.651
Q9NPJ3	ACOT13	2.221	0.699	Q9Y3Z3	SAMHD1	3.157	-1.685
O75368	SH3BGRL	2.756	0.682	Q9ULZ3	PYCARD	1.868	-1.721
Q7Z7L1	SLFN11	1.307	0.672	P04083	ANXA1	4.236	-1.997
Q16643	DBN1	1.804	0.642	O94788	ALDH1A2	3.923	-2.501
P61163	ACTR1A	1.594	0.626	Q8WVV4	POF1B	3.688	-2.577
Q5JWF2	GNAS	1.752	0.606	Q9BXV9	C14orf142	1.312	-3.599
Q9Y696	CLIC4	2.964	0.586				

Table S6C.

Proteins that were significantly differentially expressed between untreated and UV-exposed WT cells, as demonstrated by label-free proteomic analysis. ($-\log_{10}$ p value>1.3, $\log_2$ fold changes x < -0.585 (blue) and x > 0.585 (red)).

Uniprot Accession number	Gene name	-log10 p value	Log2 ΔCSNAP/WT ratio	Uniprot Accession number	Gene name	-log10 p value	Log2 ΔCSNAP/WT ratio
P68431	HIST1H3A	1.325	4.516	Q27J81	INF2	1.680	0.830
Q96P11	NSUN5	1.378	4.265	P42785	PRCP	1.406	0.822
Q14534	SQLE	1.598	3.907	O95881	TXNDC12	1.732	0.737
Q15274	QPRT	1.564	3.667	Q12788	TBL3	1.479	0.658
Q96QV6	HIST1H2AA	1.489	2.740	Q9C0B1	FTO	1.372	0.655
G3V325	ATP5J2	1.595	2.687	P00491	PNP	2.027	0.622
Q04760	GLO1	1.469	2.641	Q56VL3	OCIAD2	2.023	0.590
S4R435	RPS10	1.435	2.399	Q9UBC2	EPS15L1	1.529	-0.592
Q9Y3D6	FIS1	1.633	2.386	O43684	BUB3	1.783	-0.595
P62304	SNRPE	1.407	2.206	P49916	LIG3	1.344	-0.600
Q9NV31	IMP3	1.410	2.197	P36543	ATP6V1E1	1.539	-0.604
P49755	TMED10	1.500	1.934	Q9UQR0	SCML2	1.638	-0.609
P25787	PSMA2	1.446	1.920	P30566	ADSL	1.490	-0.620
P43307	SSR1	1.578	1.839	P41091	EIF2S3	1.403	-0.622
Q9Y2L1	DIS3	1.447	1.792	Q5VT52	RPRD2	1.822	-0.635
O75607	NPM3	1.633	1.784	Q5JRA6	MIA3	1.334	-0.639
Q9Y3C4	TPRKB	1.384	1.771	P35579	MYH9	1.846	-0.645
Q9H993	ARMT1	1.659	1.708	P62899	RPL31	1.396	-0.648
Q15067	ACOX1	1.779	1.694	P10606	COX5B	1.337	-0.648
Q9P287	BCCIP	1.667	1.640	P46108	CRK	1.527	-0.668
Q9UBT2	UBA2	1.308	1.612	O00231	PSMD11	1.637	-0.668
P49137	MAPKAPK2	2.164	1.561	P08754	GNAI3	1.323	-0.672
Q8N183	NDUFAF2	1.448	1.558	P35610	SOAT1	1.324	-0.693
P62995	TRA2B	1.757	1.540	Q9H501	ESF1	1.618	-0.708
Q9UFG5	C19orf25	1.915	1.494	Q15291	RBBP5	1.506	-0.708
P62249	RPS16	1.399	1.470	Q6IN85	SMEK1	1.351	-0.721
Q9H6F5	CCDC86	1.347	1.467	Q9NY93	DDX56	1.507	-0.722
P14174	MIF	1.506	1.462	E7EWR4	CSTF2	1.707	-0.729
P43246	MSH2	1.670	1.451	P31946	YWHAB	1.359	-0.736
P23258	TUBG1	1.470	1.317	O75822	EIF3J	1.335	-0.740
Q00013	MPP1	1.718	1.295	P52907	CAPZA1	1.893	-0.741
Q9UGR2	ZC3H7B	1.719	1.264	Q9BXS6	NUSAP1	1.473	-0.755
Q96F86	EDC3	2.623	1.254	Q9UBM7	DHCR7	1.392	-0.757
Q6P3X3	TTC27	2.116	1.232	P16220	CREB1	1.489	-0.769
P62314	SNRPD1	1.379	1.218	P49189	ALDH9A1	1.457	-0.772
Q14011	CIRBP	1.486	1.207	Q9Y520	PRRC2C	1.706	-0.775
P60903	S100A10	1.430	1.174	P35251	RFC1	1.375	-0.785
Q709C8	VPS13C	1.667	1.159	Q32MZ4	LRRFIP1	1.339	-0.792
P13995	MTHFD2	1.467	1.094	Q7Z739	YTHDF3	1.526	-0.793
Q5VUJ6	LRCH2	1.485	1.077	P62829	RPL23	1.523	-0.798
O95782	AP2A1	1.874	1.058	P60468	SEC61B	1.309	-0.800
Q5T4S7	UBR4	2.068	1.045	Q9NW13	RBM28	1.387	-0.801
P60981	DSTN	1.325	1.035	A0A0A0MRA8	EPB41L3	1.410	-0.809
Q10471	GALNT2	1.523	1.000	Q86YP4	GATAD2A	1.764	-0.821
Q14160	SCRIB	1.560	0.988	Q9NTJ3	SMC4	1.527	-0.825
O94888	UBXN7	1.314	0.987	Q99504	EYA3	1.395	-0.826
P47712	PLA2G4A	1.637	0.967	Q7Z3K3	POGZ	1.483	-0.834
Q96G61	NUDT11	1.960	0.900	Q9Y2Q5	LAMTOR2	1.348	-0.838
Q10713	PMPCA	1.484	0.896	Q02818	NUCB1	1.530	-0.847
Q9UHI6	DDX20	2.188	0.842	P17096	HMGA1	1.508	-0.851

Uniprot Accession number	Gene name	-log10 p value	Log2 ΔCSNAP/WT ratio	Uniprot Accession number	Gene name	-log10 p value	Log2 ΔCSNAP/WT ratio
Q92793	CREBBP	2.055	-0.854	A6NHR9	SMCHD1	1.368	-1.044
P50416	CPT1A	1.329	-0.880	Q69YH5	CDCA2	1.373	-1.054
Q9BT78	COPS4	2.061	-0.880	Q08170	SRSF4	1.370	-1.058
Q5HYI8	RABL3	1.455	-0.884	Q7Z417	NUFIP2	1.584	-1.059
Q14151	SAFB2	1.388	-0.888	P85037	FOXK1	1.433	-1.062
J3KQN4	RPL36A	1.424	-0.902	Q9UK76	HN1	1.334	-1.063
P27694	RPA1	1.513	-0.910	Q09666	AHNAK	1.502	-1.068
Q9H2G2	SLK	2.021	-0.913	Q15637	SF1	1.530	-1.072
P22059	OSBP	2.117	-0.916	Q13492	PICALM	1.502	-1.090
Q99543	DNAJC2	1.553	-0.916	O75694	NUP155	1.665	-1.111
P49207	RPL34	1.472	-0.929	O95674	CDS2	1.355	-1.140
P98172	EFNB1	1.557	-0.932	Q9Y5J1	UTP18	1.758	-1.150
E7ESU0	USP19	1.331	-0.935	Q9UH62	ARMCX3	1.658	-1.152
P20962	PTMS	1.682	-0.939	Q9BZI7	UPF3B	1.311	-1.171
Q8WW12	PCNP	1.305	-0.949	Q5T6F2	UBAP2	1.460	-1.179
P78527	PRKDC	1.437	-0.964	Q96A65	EXOC4	2.251	-1.180
Q9H2M9	RAB3GAP2	1.310	-0.966	O75821	EIF3G	1.324	-1.207
Q9UHD9	UBQLN2	1.373	-0.976	Q9BTX1	NDC1	2.060	-1.235
P63218	GNG5	1.336	-0.998	Q14061	COX17	1.309	-1.270
Q14008	CKAP5	1.351	-1.005	Q96R06	SPAG5	1.587	-1.287
Q13619	CUL4A	1.386	-1.008	Q02952	AKAP12	1.428	-1.298
Q9UHX1	PUF60	2.024	-1.008	Q9Y232	CDYL	1.534	-1.337
Q9H3N1	TMX1	1.576	-1.012	O00592	PODXL	1.415	-1.342
Q8NB90	SPATA5	2.533	-1.019	Q9NY61	AATF	1.693	-1.348
O14545	TRAFD1	1.582	-1.022	P46100	ATRX	1.665	-1.382
Q9BXR0	QTRT1	1.658	-1.026	Q9Y6I3	EPN1	1.808	-1.443
Q15075	EEA1	1.319	-1.027				

Table S6D.

Proteins that were significantly differentially expressed between untreated and UV-exposed ΔCSNAP cells, as demonstrated by label-free proteomic analysis. ($-\log_{10}$ p value>1.3, $\log_2$ fold changes x < -0.58 (blue) and x > 0.58 (red)).

Uniprot Accession number	Gene name	-log10 p value	log2 ΔCSNAP/WT ratio
Q12962	TAF10	1.344	2.203
O94788	ALDH1A2	1.493	0.933
Q9BXR0	QTRT1	1.336	0.853
Q9UKJ3	GPATCH8	1.384	-1.005
P20020	ATP2B1	1.461	-1.158

Table S7.

Pathway enrichment analysis of whole cell label free proteomics data.

The table is provided as a separate excel file.

Table S8.

Known CRL substrates identified in total proteome analysis of WT and ΔCSNAP cells. Color coding represents up- (red) or downregulated (blue) proteins. Based on references (1)(Emanuele et al., 2011), (2)[21], (3)[22], and (4)[23].

Differentially expressed CRL substrate proteins		References	CRL	GO Annotation / Pathway (Biological process / Molecular Function*)	
ΔCSNAP/WT	AASDHPPT	2	CRL1		
	IDH2	2	CRL1		
	HSBP1	2	CRL1		
	SQSTM1	1,2,4	CRL1, CRL2	Apoptosis Ubiquitin-dependent protein degradation	GO:0006915 GO:0006511
	WAC	2	CRL1	DNA damage response G1 DNA damage checkpoint Ubiquitin-dependent protein degradation	GO:0006974 GO:0044783 GO:0032435
	LIG3	4	CRL2	Cell cycle	GO:0007049
	GATAD2A	1,4	CRL2		
	NFATC2IP	4	CRL2		
	QTRT1	4	CRL2		
	UBE2S	4	CRL2/CRL4	Anaphase-promoting complex-dependent protein degradation Cell division Regulation of ubiquitin protein ligase activity	GO:0031145 GO:0051301 GO:1904668
	LRRC41	1,4	CRL2/CRL4	Protein ubiquitination	GO:0016567
	RBBP5	4	CRL2/CRL4	DNA damage response	GO:0006974
	PYCARD	4	CRL2/CRL4	Apoptosis	GO:0006915
	GNAS	4	CRL4A/CRL4B		
	SOAT1	4	CRL4A/CRL4B	Cholesterol homeostasis	GO:0042632
	UGP2	4	CRL4B	Glycogen metabolic process	GO:0005977
	CCNA2	3	CRL1	Cell cycle G1/S phase transition Cell division Regulation of cell cycle	GO:0044843 GO:0051301 GO:0051726
	TYMS	1			
	SERPINB6	1			
	NUP54	1			
	EIF3I	1			
	PPP2CB	1			
	HUWE1	1		Protein ubiquitination	GO:0042787
	HEATR1	1			
	HSP90AA1	1		Protein ubiquitination	GO:0031396
	DHX9	1		Regulation of DNA repair	GO:0045739
	IMPDH2	1			
	URB1	1			
	UBE4B	1		Ubiquitin-dependent protein degradation	GO:0043161
	RAD23A	1		Nucleotide-excision repair Cell cycle Ubiquitin-dependent protein degradation	GO:0006289 GO:0045787 GO:0032436
	CDYL	1			
	SAMHD1	1			

Differentially expressed CRL substrate proteins		References	CRL	GO Annotation / Pathway (Biological process / Molecular Function*)	
ΔCSNAP UV / WT UV	PDCD4	1,2,3	CRL1	Apoptosis Regulation of cell cycle	GO:0006915 GO:0045786
	IDH2	2	CRL1		
	LRRC41	1,4	CRL2/CRL4	Protein ubiquitination	GO:0016567
	PYCARD	4	CRL2/CRL4	Apoptosis	GO:0006915
	GNAS	4	CRL4A/CRL4B		
	AURKA	3	CRL1	Mitotic cell cycle	GO:0000278
	CCNA2	3	CRL1	Cell cycle G1/S phase transition Cell division Regulation of cell cycle	GO:0044843 GO:0051301 GO:0051726
	KRT8	1		Extrinsic apoptotic signaling pathway	GO:0097191
	VCL	1		Movement of cell or subcellular component	GO:0006928
	SAMHD1	1			

*GO Annotation Molecular Function